1

2 **Full title:**

3

4 Drug reformulation for a neglected disease.

5

6 The NANOHAT project to develop a safer more effective sleeping sickness drug.

7

8 **Short title:**

9 Pentamidine reformulation to improve safety and efficacy against Human African Trypanosomiasis

10

11

12 ***AUTHORS:*** *Lisa Sanderson*[1†], *Marcelo da Silva*[1†], *Gayathri N. Sekhar*[1], *Rachel C. Brown*[1], *Hollie Burrell-*

13 *Saward*[2], *Mehmet Fidanboylu*[1], *Bo Liu*[3], *Lea Ann Dailey*[1], *Cécile A. Dreiss*[1], *Chris Lorenz*[4], *Mark Christie*[1],

14 *Shanta J. Persaud*[3], *Vanessa Yardley*[2], *Simon L Croft*[2], *Margarita Valero*[5] *and Sarah A. Thomas*[1]*

15 [1]King's College London, Institute of Pharmaceutical Science, Stamford Street, London, UK

16 [2]Faculty of Infectious and Tropical Diseases, London School of Hygiene and Tropical Medicine, London,
17 UK.

18 [3]King's College London, Department of Diabetes, School of Life Course Sciences, Faculty of Life
19 Sciences & Medicine, 2.9N Hodgkin Building, Guy's campus, London UK.

20

21 [4]King's College London, Theory & Simulation of Condensed Matter Group, Department of Physics,
22 Strand, London WC2R 2LS, UK

23

24 [5]Physical Chemistry Department, Faculty of Pharmacy, University of Salamanca, Spain.

25

26

27 †Joint first authors

28

29 *Corresponding author: sarah.thomas@kcl.ac.uk

30

31

32

33 **Author Contributions for uploading during submission**

34 **LS: PDRA** *in vivo* BBB (PK and In situ brain perfusion technique) and *in vitro* BBB studies. Data analysis.
35 Result writing.

36 **MAS:** PDRA insulin secretion and cell viability studies, physical chemistry, data analysis result writing.

37 **GNS:** PhD Student *in vitro* BBB studies, haemolysis assay, membrane integrity assay. Data analysis

38 **RCB:** *in vitro* BBB studies.

39 **HBS:** PhD Student *in vitro* anti-trypanosomal assays.

40 **MF:** PhD Student contributed to the initial concept and data sets with P85.

41 **BL**: Trained MF, MAS and LS in insulin secretion assay and helped obtain preliminary data

42 **LAD:** Haemolysis assay and with SAT obtained funding from BBSRC Centre of Integrative Bioscience for
43 the use of this assay in this study.

44 **SAT:** Introduction, method, result and discussion writing, paper collation, co-ordination. CNS drug
45 delivery expert. Obtained MRC DPFS funding, concept, project management and experimental design,
46 data analysis and interpretation.

47 **CD, CL, MV, SP, MC, SC, SAT:** obtaining MRC DPFS funding, concept, project management and
48 experimental design, data analysis and interpretation.

49

Abstract

Human African trypanosomiasis (HAT or sleeping sickness) is caused by the parasite *Trypanosoma brucei sspp.* The disease has two stages, a haemolymphatic stage after the bite of an infected tsetse fly, followed by a central nervous system stage where the parasite penetrates the brain, causing death if untreated. Treatment is stage-specific, due to the blood-brain barrier, with less toxic drugs such as pentamidine used to treat stage 1. The objective of our research programme was to develop an intravenous formulation of pentamidine which increases CNS exposure by some 10-100 fold, leading to efficacy against a model of stage 2 HAT. This target candidate profile is in line with drugs for neglected diseases inititative recommendations. To do this, we evaluated the physicochemical and structural characteristics of formulations of pentamidine with Pluronic micelles (triblock-copolymers of polyethylene-oxide and polypropylene oxide), selected candidates for efficacy and toxicity evaluation *in vitro*, quantified pentamidine CNS delivery of a sub-set of formulations *in vitro and in vivo,* and progressed one pentamidine-Pluronic formulation for further evaluation using an *in vivo* single dose brain penetration study. Screening pentamidine against 40 CNS targets did not reveal any major neurotoxicity concerns, however, pentamidine had a high affinity for the imidazoline$_2$ receptor. The reduction in insulin secretion in MIN6 β-cells by pentamidine maybe secondary to pentamidine-mediated activation of β-cell imidazoline receptors and impairment of cell viability. Pluronic F68 (0.01%w/v)-pentamidine formulation had a similar inhibitory effect on insulin secretion as pentamidine alone and an additive trypanocidal effect *in vitro*. However, all Pluronics tested (P85, P105 and F68) did not significantly enhance brain exposure of pentamidine. These results are relevant to further developing block-copolymers as nanocarriers, improving BBB drug penetration and understanding the side effects of pentamidine.

Abbreviations: aqueous (aq), blood-brain barrier (BBB), critical aggregation concentration (CAC), critical micellar concentration (CMC), circumventricular organs (CVO), Cyanmethaemoglobin (CMH), developmental pathway funding scheme (DPFS), dissipative particle dynamics (DPD), Drugs for Neglected Diseases initiative (DNDi), dynamic light-scattering (DLS), human African trypanosomiasis

76 (HAT), hydrophilic-lipophilic balance (HLB), intravenous (iv), inward rectifying (IR), molecular weight
77 (MW), multi-drug resistance associated protein (MRP), Medical Research Council (MRC), not available
78 (na), parts per million (ppm), pentamidine isethionate (PTI), P-glycoprotein (Pgp), plasma free
79 haemoglobin (PFH), poly(ethylene oxide) (PEO), poly(propylene oxide) (PPO), saline (sal), scattering
80 length density (SLD).
81

Introduction

Human African trypanosomiasis (HAT or sleeping sickness) is a potentially fatal disease caused by the parasite *Trypanosoma brucei sspp*. Recent epidemiological studies in 30 of the 36 African countries listed as endemic for the disease indicate that, whilst the number of disease cases has been decreasing since 1990, there are still ~4,000 new infections/year, and ~15,000 cases worldwide [1][2]. Furthermore, there is a substantial unreported burden of HAT [3].

The disease has two stages – a haemolymphatic stage after the bite of an infected tsetse fly, followed by a central nervous system (CNS) stage when the parasite penetrates the brain, causing death if left untreated. The blood-brain barrier (BBB) makes the CNS stage difficult to treat because it prevents 99% of all known compounds from entering the brain, including most anti-HAT drugs[4][5][6][7]. Those that do enter the brain are toxic compounds, can have serious side effects, are complex to administer and/or are expensive. Pentamidine is a less toxic blood stage drug, which is known to treat early-late (transition) stage HAT[8], but cannot treat stage 2 disease as it does not sufficiently penetrate the BBB[7] and causes peripheral side effects (e.g. hypoglycaemia (incidence 5-40%) and diabetes mellitus (incidence: occasional but irreversible)[9] which preclude increasing the dose to overcome this limitation. Research has shown pentamidine has a limited ability to cross the BBB and reach the brain due to it physicochemical characteristics and its removal by the efflux transporters P-glycoprotein (Pgp) and multi-drug resistance associated protein (MRP) [7](Fig S1). Furthermore, transporters are considered essential in the mode of action of pentamidine against trypanosomes.

Poloxamers, with commercial trademark Pluronics® (BASF) or Synperonics® (CRODA), are triblock copolymers made of two poly(ethylene oxide) (PEO) blocks interspaced by a poly(propylene oxide) (PPO) block and follow the general basic formula: PEO_x-PPO_y-PEO_x, where x and y are the size of PEO and PPO blocks, respectively (Table 1). In an aqueous environment and above the critical micelle concentration (CMC), the copolymers self-assemble into micelles, with the PEO chains forming a hydrophilic shell around a PPO hydrophobic core, within which lipophilic drugs can be solubilised,

drug-free fraction decreased and circulation time increased [10]. A variety of Pluronic block copolymers differing in the lengths of the EO and PO blocks are available for formulation with pharmaceutical drugs. Importantly the size of the hydrophobic block affects micellization and drug solubilisation[11]. Furthermore, combining different Pluronics® can enhance drug/micelle interactions and drug loading[12][13]. The PEO shell serves as a stabilizing layer between the hydrophobic core and the external medium, and prevents aggregation, plasma protein adsorption and opsonization and therefore recognition by the macrophages of the reticuloendothelial system [14]. Pluronic copolymers are also endowed with low cytotoxicity and weak immunogenicity in topical and systemic administration. Even though PEO–PPO–PEO materials are non-degradable, molecules with a molecular weight (MW) <7 kDa can be filtered by the kidney and cleared in urine[15] (Table 1). In addition, Pluronics are recognised pharmaceutical excipients listed in the US and British Pharmacopoeia so have an established safety profile.

Thus Pluronics have attracted a great deal of attention in pharmaceutical applications as drug solubilisers [14] or controlled drug-release agents[16][13][17]. Notably, Pluronic P85, P105, F68 and L61 have been shown to inhibit efflux transporters (including P-gp and MRP1-2) and have potential to enhance drug passage across the BBB [18] [19][20] [21] [22][23][24][16][25][26][27]. They have all been approved as cosmetic ingredients [15] with F68 having been utilized as a blood substitute component[28]. Transporter-targeting Pluronics® (L61 and F127) have successfully completed a phase 2 clinical trial for the intravenous treatment of adenocarcinoma of the upper gastrointestinal tract [29][30]. Interestingly, F127-based amphotericin B-containing micelles have been shown to be highly effective in treating *Leishmania amazonensis*-infected BALB/c mice [31], demonstrating that Pluronics have potential beyond the traditional role of simple micellar vessels for drug encapsulation and longer circulation, but are also active agents with key biological functions [32].

132 In this Medical Research Council (MRC) developmental pathway funding scheme (DPFS) multi-
133 disciplinary study our team developed a milestone driven progression strategy (Fig 1) in order to
134 assess the potential of pentamidine-Pluronic formulations to effectively treat stage 2 disease, reduce
135 the major known side effect of pentamidine on the pancreas and shorten the length of treatment
136 required to treat stage 1 disease. It was anticipated that the benefits of this approach would be a
137 combined pentamidine-Pluronic formulation which would provide a single therapeutic entity for safer,
138 simpler and more cost-effective treatment of all HAT stages using an established drug with a known
139 safety profile. Four Pluronics were selected for evaluation based on their block-copolymer
140 architecture, established safety profile and known ability to inhibit Pgp. These were P85, P105, F68
141 and L61 (Table 1). An iterative approach was utilized as illustrated in Fig 1.
142

143 **Fig 1**. **NANOHAT project progression strategy.**
144 We screened approximately 30 pentamidine/Pluronic® formulations during this project using a
145 rational, iterative approach. The three milestones were intended to ensure that the most appropriate
146 formulations, on the basis of *in silico* and *in vitro* data, were taken forward to the *in vivo*
147 pharmacokinetic studies and that the formulations with the greatest likelihood of success would be
148 tested in the whole animal efficacy studies as outlined in the progression strategy.
149
150

151 # 2. Methods

152 ## 2.1a Materials

153 Pentamidine (1,5-bis-4ρ-amidinophenoxypentane) isethionate salt (MW 592.68; 98% purity; catalogue
154 number P0547) and Pluronic P105 (batch number BCBP8915V) were purchased from Sigma Aldrich
155 (Poole, Dorset, UK). Pluronic P85 (mat 30085877 batch number: WPYE5378) was a kind donation from
156 BASF plc (Cheshire, UK). Pluronic F68 (medical grade Catalogue number 2750016; batch numbers
157 M7102 and MR29468) was purchased from MP Biomedicals, LLC (Illkirch Cedex, France). L61 was
158 purchased from Aldrich (catalogue number 435422; batch number MKBH8737V).

159

160 ## 2.1b Purity of excipients

161 All Pluronic formulations (F68, P105, P85 and L61) were tested for possible contamination due to the
162 synthesis process and met specifications established by the US Pharmacopeia convention NF32
163 monograph for polaxamers [15], in that the EO, PO and p-dioxane in the Pluronic were below 1, 5 and
164 5 parts per million (ppm), respectively. This analysis was performed by an external specialist
165 laboratory (Butterworth laboratories, Teddington, UK).

166

167 **Table 1. Pluronics used in this Study, with their Name, Block Composition, Hydrophilic-Lipophilic**
168 **Balance (HLB) and General Formula. L, F, or P, Refers to Liquid, Flake, or Paste Physical Forms,**
169 **respectively.**

Poloxamer	Pluronic	MW	Number of EO blocks	Number of PO blocks	HLB	Formula
235	P85	4600	52.27	39.66	16	$EO_{26.13}PO_{39.66}EO_{26.13}$
335	P105	6500	73.86	56.03	15	$EO_{36.93}PO_{56.03}EO_{36.93}$
188	F68	8400	152.73	28.97	29	$EO_{76.37}PO_{28.97}EO_{76.37}$
181	L61	1950	4.55	31.03	3	$EO_2PO_{30}EO_2$

170

171 ## 2.2 Evaluation of potential neurotoxicity of pentamidine

172 New toxicities may arise following pentamidine's improved access to the CNS. The potential of
173 pentamidine to cause neurotoxicity was evaluated by a brief review of the literature together with a
174 neurological profiling screen and ion channel activity screens. The biological screens were performed
175 by external specialist laboratories as described below.
176
177 **2.2a Neurological profiling screen.** A CNS side effect panel was custom designed and binding assays
178 performed by Perkin-Elmer Science Discovery Systems (Hanover MD 21076, USA). Testing was
179 performed at a single concentration of 1 μM (100-times the trypanocidal concentration), with follow
180 up concentration-response curves in any assay where there was greater than 70% inhibition to
181 determine an inhibition constant (K_i).
182
183 **2.2b Ion channel (hKir2.1) activity screens.** The *in vitro* effects of pentamidine isethionate on cloned
184 hKir2.1 potassium channels (encoded by the human KCNJ2 gene) responsible for the I_{K1}, inwardly
185 rectifying potassium current, were examined by ChantTest Corporation (Cleveland Ohio 44128, USA)
186 to industry standards (Chantest FastPatch Assay; study number. 130827.DCC). Human epithelial
187 kidney 293 (HEK293) cells (ATCC, Manassas VA USA) were stably transfected with the appropriate ion
188 channel cDNA encoding the pore-forming channel unit. Cells were cultured in Dulbecco's Modified
189 Eagle Medium / Nutrient Mixture F-12 (D-MEM/F-12) supplemented with 10% fetal bovine serum, 100
190 U/mL penicillin G sodium, 100 μg/mL streptomycin sulphate and 500 μg/mL G418. Cultured cells were
191 maintained in a tissue culture incubator set at 37°C in a humidified 95% air and 5% CO_2 atmosphere.
192 Pentamidine was dissolved in HEPES-buffered physiological saline containing 0.3% DMSO and
193 sonicated (Model 2510/5510, Branson Ultrasonics, Danbury, CT) at room temperature for at least 20
194 minutes. A glass-lined 96 well compound plate was loaded with the appropriate amount of test (five
195 different concentrations) and positive control (100μM $BaCl_2$) solutions, and placed in the plate well of
196 the QPatchHT (Sophion Bioscience A/S, Denmark). All experiments were performed at room
197 temperature. Each cell acted as its own control. Vehicle was applied to naïve cells for a 5-10 minute

198 exposure interval. The test solution applied for a minimum of three minutes via the QPatch robot
199 pipetting system to naïve cells (n≥2, where n=the number of cells/concentration). Each solution
200 exchange on the QPatch, performed in quadruplicate, consisted of a 5 μl exchange through the
201 microfluidic flow channel, resulting in 100% replacement of the compound in the QPlate. Intracellular
202 solution was loaded into the intracellular compartments of the QPlate planar electrode (130mM K-
203 Asp, 5mM $MgCl_2$, 5 mM EGTA, 4mM Tris-ATP and 10 mM HEPES). Cell suspension was pipetted into
204 the extracellular compartments of the QPlate planar electrode.
205
206 Onset and steady state block of hKir2.1current was measured using a ramp protocol with fixed
207 amplitudes (hyperpolarization: -110 mV, 200 ms duration, followed by a 1-second ramp from -110 mV
208 to +50 mV) repeated at 10 s intervals from a holding potential of –70 mV. Current amplitude was
209 measured at the end of the step to -110 mV. Leak current was calculated and subtracted from the
210 total membrane current record.
211

212 **2.3 Determination of the micellar aggregation properties of Pluronic**

213 The CMC, micellar size and aggregation number were determined in different solvents, using a unique
214 combination of light and neutron scattering and atomistic simulations. We also measured the
215 partitioning of pentamidine isethionate in selected Pluronic and the *in vitro* release profile.
216
217 **2.3a Preparation of solutions for physicochemical measurements** Unless stated, F68, P85, P105 or
218 L61 were either dissolved in water (aqueous) or saline solution (0.9% w/v sodium chloride solution).
219 Pluronic mixtures were also prepared either with a fixed mass ratio of 1:1 (F68-P105 or F68-P85) or in
220 the case of L61, 0.01%. Samples were left to equilibrate for at least 3 hours prior to any
221 measurement. Ultra-pure water (18.2 MΩ·cm - Millipore-filtered) was used throughout the
222 experiments.
223

224 **2.3b: Phase behaviour.** In this study, L61 alone and in mixtures with one or two other Pluronics in
225 both water (aqueous) and saline mediums were visually assessed from 20°C to 50°C in 5°C steps, plus
226 37°C, to assess the impact of mixtures on L61 cloud point (24°C for a 1% solution) [33].

227

228 **2.3c CMC determination by fluorescence spectroscopy.** The CMC determines thermodynamic stability
229 of the micelles during dilution of the drug delivery system in body fluids[17][11]. Furthermore, CMC is
230 an important parameter in view of the biological response modifying effects of Pluronic block
231 copolymers since it is needed to determine the maximum achievable concentration of the polymer
232 single chains ("unimers") [20]. For measurement of the CMC, pyrene (Sigma catalogue number 82648;
233 pyrene puriss p.a. for fluorescence, ≥99%) was used as a probe. A stock solution of pyrene in acetone
234 (1.7×10^{-2} M) was initially prepared. A 35 µL aliquot of this solution was placed in a 100 mL volumetric
235 flask and the solvent was evaporated to air. The residue was then dissolved in either ultra-pure water
236 (18.2 MΩ·cm - Millipore-filtered) or 0.9% w/v sodium chloride solution, resulting in a final
237 concentration of pyrene of 6×10^{-6} M. These solutions were then subsequently used as the solvent for
238 the polymer solutions. Stock solutions of each Pluronic in water and saline solution were prepared. An
239 appropriate aliquot of these solutions were dissolved in the pyrene/H_2O or pyrene/saline solution.
240 Solutions of different polymer concentration were obtained by diluting the stock polymer solution
241 with the appropriate solvent. Mixed samples of two Pluronics were also prepared either with a fixed
242 ratio of 1:1 or containing 0.01% L61. Samples were left to equilibrate for at least 3 hours prior to the
243 experiment.

244 The fluorescence emission spectra were recorded on a Cary Eclipse fluorescence spectrophotometer
245 (Varian, Oxford, UK) with λ_{exc} = 340 nm. For the CMC, fluorescence intensities at 373, 384, 393 nm and,
246 when it appeared, also at the excimer band centred at 490 nm, were measured. For each polymer, the
247 critical aggregation concentration value was determined by using the intensity of the best resolved

248 peak. At least two repeats were performed for each sample. Measurements were performed at 20°C

249 and 37°C.

250

251 **2.3d Stability testing** The purpose of stability testing is to check whether pentamidine becomes

252 altered with time under the influence of a variety of environmental factors such as temperature,

253 humidity and light (Climatic zone IV, 30°C and 65-75% relative humidity) [34].

254

255 In our initial 7 day assessment we also considered interaction of pentamidine with Pluronic as

256 product-related factors may also influence its quality. A 5% or more change in initial content of

257 pentamidine was considered significant. Pentamidine concentration at day 0, 10 and 7 was assessed

258 by NMR.

259 A Bruker Advance 400 MHz spectrometer was used for recording the one-dimensional (1D) 1H NMR.

260 Solutions of PTI, PTI/P85, PTI/P105 and PTI/F68 were prepared in D_2O (≥99.85% in deuterated

261 component). Data were collected at days 0, 1 and 7. Samples were stored in amber NMR tubes at

262 37°C.

263

264 **2.3e Partition coefficient determination.** The partitioning coefficient, *P*, determines the fraction of

265 drug incorporated into the micelle and provides thermodynamic characterization for the stability of

266 the drug-micelle complex during dilution within the body fluids[17][11].

267 The partition coefficient of pentamidine in the micellar core and bulk solvent, as described by Kabanov

268 and co-workers [11], was measured for F68, P105 and mixtures of P105 and F68 (1:1), in both saline

269 and aqueous solutions and at 20°C and 37°C.

270

271 The partition coefficient was obtained following the procedure described by Kabanov and co-workers

272 [11], which is described briefly below. The partition coefficient is defined as:

273 $$P = \frac{c_m}{c_{bulk}}$$ Eq. 1

274 where c_m is the PTI concentration in the micelle core and c_{bulk} is the PTI concentration in the

275 bulk solvent.

276 The partition coefficient P can be obtained from[11]:

277 $$P = \frac{1}{0.01*\alpha*v}$$ Eq. 2

278 where, v (cm^3/g), the partial molar specific volume, is defined as:

279 $$v = \frac{1}{\rho_0} * \frac{1-(\rho_s-\rho_0)}{C}$$ Eq. 3

280 with ρ_0 ($g{\cdot}cm^{-3}$) the solvent density, ρ_s ($g{\cdot}cm^{-3}$) the density of the solution and C the polymer

281 concentration ($g{\cdot}mL^{-1}$).

282 α is defined as the angular coefficient of the plot $(\frac{I-I_0}{I_{max}-I_0})^{-1}$ vs. (Pluronic concentration – cac)$^{-1}$, where I

283 is the fluorescence intensity of the solution, I_0 is the intensity with no Pluronic present and I_{max} is the

284 intensity at saturating concentration of the Pluronic, cac the critical aggregation concentration.

285

286 For the measurement of pentamidine isethionate salt (PTI) partition coefficient, a PTI 1×10^{-6} M in both

287 water and saline solutions were initially prepared. These solutions were then subsequently used as

288 the solvent for the polymer solutions and the preparation followed a similar method as for the CMC

289 measurements. Samples were left to equilibrate for at least 3 hours prior to the experiment.

290

291 The fluorescence emission spectra were recorded on a Cary Eclipse fluorescence spectrophotometer

292 (Varian, Oxford, UK) with $\lambda_{exc} = 260$nm, for pentamidine. The fluorescence emission intensity at ca

293 340 nm was followed.

294 **2.3f Drug release.**

295 Solutions of Pluronic (1% F68 and 1% P105) with 10 mM PTI and PTI alone in water (2 mL) were loaded

296 into 2 mL mini-dialysis tubes with 1 kDa molecular weight cut-off (GE Healthcare Bio-sciences Corp.

USA). The tube was immersed in a 200 mL closed Duran flask which was placed in a water bath at 37°C for the duration of the experiment. Aliquots were collected from the immersion water (ultra-pure water (18.2 MΩ·cm - Millipore-filtered) in the flask every 30 min for the first 2 hours, every hour for the next 5 hours and then once more after 1 week. At the end of the experiment, an aliquot was collected from the dialysis cell. PTI concentrations were determined by UV spectroscopy (wavelength 260 mm).

The data was fitted to Ritger-Peppas model[35].

$$\frac{M}{M_{\infty}} = kt^{n} \qquad \text{Eq. 4}$$

Where M and M_{∞} are the cumulative amounts of drug released at time t and at infinite time, respectively; k, the reaction constant, t the time, n, the diffusional exponent describing the type of regime type: n=1, case II transport, n=0.5, Fickian diffusion, $0.5<n<1$ non-Fickian diffusion.

2.3g Dynamic light scattering (DLS).

Dynamic light-scattering (DLS) were performed with a photon correlation spectrometer Malvern Zetasizer Nano with a laser wavelength of 633nm. For obtaining the reduced scattered intensity, toluene was used as the standard and the increment in the refractive index, $\partial n/\partial c$, was assumed to be independent on the temperature and taken as 0.133 ± 0.002 $mL \cdot g^{-1}$ [36]. The samples, of concentrations ranging between 1 to 5% w/v, were filtered prior to the measurements by 0.22 μm Millex syringe PVDF filters onto semi-micro glass cells. The temperature of the sample was controlled with 0.1°C accuracy by the built-in Peltier in the cell compartment. Size distributions were obtained for each sample from the analysis of the intensity autocorrelation function, which was performed with the Zetasizer software in the high resolution mode to distinguish overlapping distributions.

322 **2.3h Small-Angle Neutron Scattering (SANS).** The architecture of the nanocarriers was measured by
323 SANS. The aggregation number (N_{agg}) and radius micellar size, including volume of core and shell
324 region, correlates directly with are relevant to properties such as drug loading encapsulation
325 efficiency, stability, half-life and hence circulation time[37].

326 Small-angle neutron scattering experiments were performed on the LOQ instrument at ISIS
327 pulsed neutron source (ISIS, Rutherford-Appleton Laboratory, STFC, Didcot, Oxford). LOQ uses
328 incident wavelengths from 2.2 to 10.0 Å, sorted by time-of-flight, with a fixed sample-
329 detector distance of 4.1 m, which provided a range of scattering vectors (q) from 0.009 to
330 0.29 $Å^{-1}$.

331 The samples used in the SANS experiments were prepared in D_2O to optimise the contrast with the
332 protonated polymer. The samples were placed in clean disc-shaped quartz cells (Hellma) of 1 and 2
333 mm path length and the measurements were carried out at 25°C and 37°C. All scattering data were
334 first normalised for sample transmission and then background-corrected using a quartz cell filled with
335 D_2O (this process also removes the inherent instrumental background arising from vacuum and
336 windows) and finally corrected for the linearity and efficiency of the detector response using
337 instrument-specific software package. The data were then converted to the differential scattering
338 cross-sections (in absolute units of cm^{-1}) using the standard procedures at ISIS [38,39].

339 The curves were fitted to a core-shell sphere model combined with a structure factor for hard
340 spheres, implemented in the Sasview software [40]. The initial fitting assumptions were a dry PPO
341 core, i.e., the scattering length density (SLD) for the core was set to the SLD of PPO (3.44×10^{-7} $Å^{-2}$), the
342 solvent as D_2O (SLD of 6.38×10^{-6} $Å^{-2}$) and the shell as dry PEO (SLD 6.4×10^{-7} $Å^{-2}$). The SLD of core and
343 solvent were kept fixed while the shell was left to vary as a high level of hydration of PEO is expected,
344 as a result, the returned SLD should be an intermediate value between D_2O and PEO. After obtaining a
345 stable set of parameters, the SLD of the core was also let free to vary. Input values for the core radius
346 and shell thickness were based on hydrodynamic radius values obtained by DLS. A term to

347 compensate for polydispersity was included for Pluronic (around 0.20), as well as a structure factor
348 ($S(q)$), corresponding to a hard sphere model, in order to account for intermicellar interactions.
349 Assuming that the shell SLD is a linear combination of the EO SLD and D_2O SLD, i.e., the densities are
350 additive, it is possible to calculate the solvent volume fraction in the shell using the following
351 expression:

352 $$\chi_{\mathrm{solv}}=\frac{SLD_{shell}-SLD_{EO}}{SLD_{D_2O}-SLD_{EO}}$$ Eq. 5

353 The amount of solvent molecules in the shell than can be obtained from the ratios of the shell volume
354 by the solvent molecular volume weighted by the solvent volume fraction:

355 $$n_{D_2O}=\frac{\chi_{solv}\cdot V_{shell}}{V_{D_2O}}$$ Eq. 6

356 Furthermore, the total micelles volume is the sum of both Pluronics and D_2O molecular volumes
357 weighted by their respective volume fractions. Therefore, combining the total micelle volume (shell +
358 core) minus the solvent contribution, it is possible to obtain the amount of Pluronic molecules present
359 in the micelle and calculate the aggregation number of the micelles.

360 $$N_{agg}=\frac{V_{micelle}-\chi_{solv}V_{shell}}{V_{pluronic}}$$ Eq. 7

361 The molecular volume of the Pluronic was approximated from the Pluronic molar volume ($v_{pluronic}$) in
362 water.

363 $$V_{pluronic}=\frac{v_{pluronic}}{N_{AV}}$$ Eq. 8

364

365 **2.3i Simulations of Pluronic self-assembly and pentamidine encapsulation.** During the course of this
366 project, we worked to develop a model of the Pluronic and pentamidine systems that would allow us
367 to simulate the self-assembly of the polymers and the encapsulation of the drugs. In order to simulate
368 the timescales and system sizes required to study these systems, we utilized a coarse-grain approach;
369 dissipative particle dynamics (DPD)[41]. This method has been used to study Pluronic before and has
370 been shown to represent expected phenomena well. So we used the simulation parameters from [42].
371

372 **2.4 Evaluation of potential peripheral toxicity of pentamidine ± Pluronic**

373 The toxicity of pentamidine in the presence of the Pluronic was explored using a variety of assays.
374 These included haemolysis, insulin secretion and membrane integrity assays.

375

376 **2.4a Haemolytic effects on human blood samples**

377 The proposed route of administration for our Pluronic formulations with pentamidine was intravenous,
378 hence the propensity for Pluronic to lyse red blood cells was studied using a haemolytic assay.

379

380 **2.4ai Chemicals.** Cyanmethaemoglobin (CMH) reagent, haemoglobin standard, Ca^{2+}/Mg^{2+} free
381 Dulbecco's Phosphate Buffered Saline (DPBS), DMSO, and Triton X-100 were purchased from Sigma-
382 Aldrich, Dorset, UK.

383

384 **2.4aii Research Donor Blood.** Healthy volunteer blood samples were drawn under the guidelines of
385 the Research Ethics Committee South East London REC 4 (10/H0807/99). Blood was collected in BD
386 vacutainer tubes containing lithium heparin as anticoagulant. Blood samples from two healthy
387 volunteers were collected and kept separate.

388

389 **2.4aiii Haemolysis Assay.** The assay is based on the protocol detailed by [43]. In order to determine
390 the total blood haemoglobin, the CMH method was used to map a standard curve based on the
391 absorption wavelength at 540 nm. Nine calibration standards were produced by preparing a stock
392 solution of 5 mg/ml (standard 1) using haemoglobin standards in CMH reagent and serially diluting it
393 to produce further standards of concentrations 2.5, 1, 0.80, 0.40, 0.20, 0.10, 0.05, and 0.025 mg/ml.
394 10% Triton X-100 (v/v) was prepared using distilled water to be used as the positive control. A 0.05%
395 solution of DMSO was prepared using distilled water and used as one of the negative controls. 0.9%
396 saline was another negative control. Pluronic samples were prepared in 0.9% saline. The test
397 concentrations of Pluronic (P85, P105 or F68) used were 0.01%, 0.1%, 0.25%, 1% or 5%.

398

399 A 5 ml vial of whole blood was centrifuged at 800 g for 15 minutes at room temperature. The
400 supernatant was removed and the remainder was used to determine the plasma free haemoglobin
401 (PFH) concentration.

402

403 200 µl x 2 of each of the calibration standards prepared were then transferred onto the 96-well plate
404 and 200 µl x 4 of CMH reagent (control 1). Total blood haemoglobin (TBH) was then prepared by
405 adding 20 µl of the whole blood with 5 ml of CMH reagent. 200 µl x 6 of TBH was transferred to the
406 plate. 6 other wells were filled with 100 µl of plasma to which 100 µl of CMH reagent was added. After
407 shaking it gently for a few minutes, the absorbance was read at 540 nm. Once the total haemoglobin
408 concentration was adjusted to 10 mg/ml using Ca^{2+}/Mg^{2+} free DPBS, 20 µl x 3 of the blank (control 2
409 0.9% saline), positive control, negative control, or Pluronic samples were added to Eppendorf tubes.
410 160 µl of Ca^{2+}/Mg^{2+} free DPBS and 20 µl of whole blood were then added to each tube except for one.
411 20 µl of Ca^{2+}/Mg^{2+} free DPBS was added instead. These served as control 3 without any blood enabling
412 us to determine any interactions from Pluronic with the assay. These tubes were incubated for 3 hours
413 ± 15 minutes in a temperature-controlled shaker (THERMOstar, BMG labtech, Offenburg, Germany) at
414 37 °C and 120 rpm. After the incubation, these were centrifuged at 800 × g for 15 minutes at room
415 temperature. 100 µl of the test samples and the controls were transferred to the 96-well plate. 100 µl
416 of CMH reagent was added to all these before measuring the absorbance spectrophotometrically at
417 540 nm. Using the calibration curve mapped earlier, the haemoglobin concentration in each of the
418 wells was determined. The dilution factor of 18 was also considered when calculating the
419 haemoglobin concentration. Haemoglobin concentration was converted to percentage haemolysis
420 compared to the negative control 0.05% DMSO. A significant increase compared to control at the 5%
421 level was taken as positively haemolytic.

422

423 **2.4b Membrane integrity/cytotoxicity.**

424 Method is described as part of 2.5b and 2.6.

425

426 **2.4c Insulin secretion and beta-cell viability.**

427 All tissue culture reagents were purchased from Sigma Aldrich (Poole, Dorset, UK).

428 Peripheral toxicity of pentamidine/Pluronic formulations to the endocrine pancreas was evaluated by

429 quantifying β-cell viability and insulin secretion from the mouse MIN6 β-cell line [44].

430

431 MIN6 β-cells were maintained in culture at 37°C (95% air/5% CO_2) in DMEM supplemented with 10%

432 fetal bovine serum, 2mM L-glutamine and $100U.ml^{-1}/0.1mg/ml^{-1}$ penicillin / streptomycin, with a

433 change of medium every 3 days. Cell were trypsinised (0.1% trypsin, 0.02% EDTA) when

434 approximately 70% confluent and seeded into 96 well plates at a density of $3x10^4$ cells/well. After a 24

435 hour culture period to allow cells to adhere, the wells were washed with PBS and cells were pre-

436 incubated for 2 hours in DMEM supplemented with 2mM glucose after which the medium was

437 replaced with DMEM supplemented with Pluronic, pentamidine and Pluronic/pentamidine solutions.

438

439 The following formulations were evaluated: F68/PTI, P85/PTI and P105/PTI with Pluronic

440 concentrations of 0, 0.01, 0.025, 0.1 and 0.5% w/v and PTI concentrations of 0, 1, 10 and 100 μM (20

441 formulations in total, including controls, Pluronic only, PTI only and solvent only were used). The cells

442 were incubated under each treatment condition for 24 hours and then evaluated for their capacity to

443 secrete insulin in response to 30 minute stimulation in the presence of 10 μM forskolin and 100 μM

444 IBMX. Insulin secretion was measured by RIA [45]. The effect of the formulations on β-cell viability

445 was assessed by determining the access of trypan blue to the cell interior, indicative of a compromised

446 plasma membrane[46].

447

448 **2.5 Blood-brain barrier studies**

449 **2.5a Radiochemicals**

450 [^{3}H(G)]pentamidine (specific activity, 31.9 Ci/mmol; concentration, 10.74 μg/ml; radiochemical purity,
451 99.4%; MW 342.64) was custom synthesized and [^{14}C(U)]sucrose (specific activity, 536 mCi/mmol;
452 concentration, 67.07 μg/ml; radiochemical purity, 98.7%) was purchased from Moravek Biochemicals,
453 California, USA.

454

455 **2.5b *In vitro* permeability assays**

456 Several *in vitro* BBB models were evaluated for this study including Caco2 (permeability format),
457 hCMEC-D3 (accumulation format), bEnd-3 (accumulation format) and MDCK-MDR (accumulation
458 format) cell lines, before selecting the MDR1-MDCK cells (permeability format) as the most
459 appropriate tool to address our objectives. MDR1-MDCK cells originate from transfection of Madin-
460 Darby canine kidney (MDCK) cells with the MDR1 gene, the gene encoding for the human efflux
461 protein, P-glycoprotein (P-gp). Using MDR1-MDCK cells avoids the complexities of multiple
462 transporters by focusing specifically on P-gp.

463 **2.5bi Preparation of formulation** 1% (w/v) stock solutions of each Pluronic and 10 mM pentamidine
464 isethionate were prepared in Hank's Balanced Salt Solution (HBSS) containing 25 mM HEPES and 4.45
465 mM glucose, at pH 7.4. These were further diluted to give final concentrations of 0.01, 0.1 or 0.5%
466 (w/v) Pluronic containing 10 μM pentamidine isethionate. Formulations were stored at room
467 temperature for 2-4 days prior to use.

468 **2.5bii *In vitro* permeability assays.** MDR1-MDCK cells (NIH, Rockville, MD, USA) were maintained and
469 permeability assays were performed at both Cyprotex (Macclesfield, Cheshire, UK) and King's College
470 London. Analysis was by UPLC-MS/MS or liquid scintillation counting as appropriate.

471 Transmission electron microscopy confirmed appropriate cell morphology of a monolayer with
472 microvilli on the apical membrane and Western blot confirmed expression of P-gp (data not shown).

473 3.4 x 10^5 cells/cm^2 were seeded on Multiscreen™ plates with 0.4 μ polycarbonate Isopore™
474 membranes (Millipore, MA, USA) in DMEM/High glucose (Sigma-Aldrich, UK , D6429) media containing
475 1% Non-Essential Amino Acids and 10% foetal calf serum (both from Sigma-Aldrich, UK). Plates were
476 maintained at 37°C/5% CO_2 for 4 days before use. On the day of the assay, DMEM was removed and
477 both the apical and basolateral surfaces of the cell monolayer were washed twice with transport
478 medium consisting of HBSS containing 25 mM HEPES and 4.45 mM glucose, (pH 7.40; 37°C). Plates
479 were incubated for 40 minutes at 37°C/5% CO_2 to stabilize physiological conditions. Transport buffer
480 was removed from the apical or basolateral chamber and replaced with the formulation to be tested.
481 Samples were taken from the apical and basolateral compartments after 1 hour of incubation at 37
482 °C/5% CO_2. Samples, including the test formulation added to the apical chamber at t=0 were analysed
483 at Cyprotex using UPLC-MS-MS method to quantify the pentamidine isethionate content or were
484 analysed for radioactivity using a Tricarb 2900TR liquid scintillation counter.

485 **2.5biii UPLC-MS/MS.** Quantification of pentamidine isethionate was carried out on an ABSciex
486 API5500 QTrap triple quadrupole mass spectrometer coupled to an Agilent 1290 Infinity UPLC system.
487 A 10μl sample from the apical or basolateral chamber was diluted with 80 μl buffer and 160 μl
488 methanol and centrifuged for 20 minutes at 1,400 × *g*. After centrifugation 90 μl of this was removed
489 and diluted with 10 μl of the internal deuterated standard to give a final concentration of 10 nM. This
490 was injected onto an Acquity™ HSS T3 (1.8 μm) column 2.1 x 50 mm (Waters Ltd, Herts, UK),
491 equilibrated at 70 °C. Separation was carried out by gradient elution using a mixture of 0.1% formic
492 acid in H_2O (solvent A) and 0.1% formic acid in acetonitrile (solvent B), at a flow rate of 600 μL/min.
493 Upon injection (10 μl), the mobile phase was held at initial conditions of 100% solvent A for 0.05
494 minutes, the concentration of solvent B was then increased to 95% at 1.00 minute post-injection using
495 a linear gradient and held for a further 0.40 minutes. The mobile phase was then returned to 100%
496 solvent A at 1.41 minutes and held for a further 0.39 minutes. The eluent was analysed by MS/MS
497 under positive ion electrospray mode and the multiple reaction monitoring transitions for

498 pentamidine and deuterated pentamidine were 341.174 to 119.984 m/z and 345.212 to 120.028 m/z
499 respectively. Calibration curves were prepared using pentamidine and the internal standard over a
500 concentration range of 0.0078 to 12 µM. The column was washed with a weak wash: 9:1 H_2O: MeCN
501 and strong wash: 4:3:3 MeOH: isopropyl alcohol: acetone + 1% acetic acid between samples.

502

503 **2.6 Sensitivity of MDCK-MDR cells to Pluronic**

504 Permeability assay with 5 µCi (0.9 µM) [^{14}C(U)]sucrose alone in the presence of varying concentrations
505 of Pluronic was used to assess the effect of Pluronic on monolayer integrity. Sucrose is a paracellular
506 permeability marker and therefore any effects of Pluronic will lead to increased diffusion of
507 [^{14}C(U)]sucrose from apical to basolateral chambers as a result of compromised BBB integrity. The
508 assay was carried out for an hour in the apical to basolateral direction only and the P_{app} of
509 radiolabelled sucrose determined at the end of the assay. Control for the assay was HBSS buffer alone.

510

511 ***2.7 In situ* perfusions**

512 The *in situ* brain/choroid plexus perfusion method for examination of the distribution of molecules
513 into the brain and CSF is an established technique in the rat, guinea-pig and mouse [47][6][48]. It
514 allows the passage of slowing moving molecules across the blood-brain and blood-CSF barriers to be
515 examined and quantified in brain, capillary endothelial cells and choroid plexus tissue for perfusion
516 periods up to 30 minutes.

517

518 **2.7a Preparation of formulation**: All formulations were prepared on the day of experiment at a
519 Pluronic concentration of 0.1, 1.0 or 5% (w/v) using artificial plasma as a diluent. The artificial plasma
520 consisted of a modified Krebs-Henseleit mammalian Ringer solution containing; 117 mM NaCl, 4.7 mM
521 KCl, 2.5 mM $CaCl_2$, 1.2 mM $MgSO_4$, 24.8 mM $NaHCO_3$,1.2 mM KH_2PO_4, 39 g dextran, 1 g/L of bovine

522 serum albumin and 10mM glucose. [^{3}H(G)]pentamidine was added to give a final concentration of

523 157nM (equivalent to 5 μCi/ml). All formulations were stirred at room temperature for at least 1

524 hour to allow any chemical interactions and micelle formation to stabilize.

525 **2.7b Animal studies:** Adult male BALB/c mice were purchased from Harlan UK Ltd (Oxon, UK). All

526 animals were maintained under standard temperature/lighting conditions and given food and water

527 *ad libitum*. Only mice above 23g in weight were used for experiments which were carried out within

528 the framework of the Animals Scientific Procedures Act (1986) and Amendment Regulations 2012 and

529 with consideration to the ARRIVE guidelines. The study was approved by the King's College London

530 Animal Welfare and Ethical Review Body.

531

532 **2.7c *In situ* perfusions.** [^{3}H(G)]pentamidine formulations were delivered to the brain using an *in situ*

533 brain perfusion technique as previously described [6]. Briefly, mice were anaesthetized (mixture of 2

534 mg/Kg Domitor™/150 mg/Kg ketamine administered via the intraperitoneal route) and heparinized

535 (100 U ip.). Oxygenated artificial plasma (described above) at 37°C was pumped via a 25 gauge

536 cannula into the left ventricle of the heart, with the right atrium severed to prevent recirculation.

537 Pumps were calibrated to deliver an overall flow rate of 5 ml/min from the cannula.

538 [^{3}H(G)]pentamidine formulations (maintained at room temperature) were fed into the flow line from a

539 dual syringe infusion pump (Harvard Apparatus, UK), at a rate of 0.5 ml/min such that the formulation

540 was diluted 1/10 immediately prior to entering the heart. 11 μM [^{14}C(U)]sucrose in artificial plasma

541 (equivalent to 5 μCi/ml) was simultaneously fed into the flow line from a second identical syringe

542 using the same pump set at 0.5 ml/min (equivalent to 1.1 μM or 0.5 μCi/ml entering the heart from

543 the cannula). The perfusion was terminated at 10 minutes or 30 minutes, and the brain was sectioned

544 as previously described [49]. Samples taken were those known to be invaded by parasites during

545 second stage sleeping sickness and/or those which control mechanisms that are disrupted by the

546 disease such as the sleep/wake cycle[6]. All samples were solubilized with 0.5 ml Solvable™

547 (PerkinElmer Life and Analytical Sciences, Buckinghamshire, UK) for 48 hours. Scintillation fluid (3.5 ml
548 Luma Safe, PerkinElmer Life and Analytical Sciences) was added and radioactivity (^{3}H and ^{14}C) was
549 counted on a Packard Tri-Carb2900TR scintillation counter in dual-label mode.

550 2.7d **Capillary depletion.** After the required samples were taken, the remaining brain tissue was
551 homogenized and analyzed by the capillary depletion method described by Thomas & Segal [50]. This
552 method uses dextran density gradient centrifugation to produce a vascular endothelial cell-enriched
553 pellet and a brain parenchyma-containing supernatant from homogenized brain tissue. Thus the
554 partitioning of a drug between the endothelial cells and the post-vascular brain parenchyma can be
555 examined [51]. Briefly, the brain tissue was weighed and homogenized in a Dounce homogenizer with
556 3 ml/g capillary depletion buffer [51] and 4 ml/g 26% dextran. The homogenate was separated by
557 centrifugation at 5,400g and 4°C for 15 minutes. Homogenate, pellet and supernatant samples were
558 solubilized and counted for radioactivity using the method described above.

559 **2.7e Expression of results.** The radioactivity (either ^{3}H or ^{14}C) present in tissue samples (dpm/g) was
560 expressed as a percentage of that measured in the artificial plasma (dpm/ml) and was termed R_{TISSUE}%,
561 as previously described [49]. Where stated, measurements for [^{3}H(G)]pentamidine were corrected for
562 the contribution of drug present in the vascular space by subtraction of the R_{TISSUE}% for [^{14}C(U)]sucrose
563 from the R_{TISSUE}% of [^{3}H(G)]pentamidine and these corrected values were termed $R_{CORR\ TISSUE}$%.

564 **2.8 Pharmacokinetic brain distribution experiments**

565 ***2.8a In vivo*** **pharmacokinetic experiments with [^{3}H(G)]pentamidine.** Formulations containing 0.025%
566 F68 with 8 μM [^{3}H(G)]pentamidine, 0.5% F68 with 8 μM [^{3}H(G)]pentamidine and 8 μM
567 [^{3}H(G)]pentamidine alone were prepared in 0.9% sterile saline and allowed to equilibrate at room
568 temperature for at least 1 hour before use. A 200 μl bolus of the formulation to be tested (equivalent
569 to 15 μCi [^{3}H(G)]pentamidine) was administered to mice via the tail vein. At 2 hours post-injection,
570 mice were exsanguinated via the right atrium of the heart into a heparinised syringe then perfused for

571 2.5 minutes with [^{14}C(U)]sucrose (1.1 μM, 0.5 μCi/ml) via the left ventricle, (all mice were
572 anaesthetised with Domitor™/ketamine and heparinised 20 minutes prior to exsanguination). Whole
573 blood samples were immediately centrifuged for 15 minutes at 5,400 × g to remove red blood cells
574 and the resulting plasma was placed on ice. A CSF sample was taken from the cisterna magna, the
575 IVth ventricle choroid plexus and pituitary gland were collected and the brain was sectioned into right
576 brain and left brain (both comprising frontal cortex and caudate putamen), cerebellum and midbrain
577 (including pons and hypothalamus). The remaining brain (including occipital cortex and hippocampus)
578 was used for capillary depletion analysis and all brain, circumventricular organs (CVO) and plasma
579 samples were solubilized and subjected to dual label (^{3}H/^{14}C) scintillation counting as previously
580 described.

581 ***2.8b In vivo*** **pharmacokinetic experiments with pentamidine isethionate.** Adult female CD1 mice
582 (20-25g) were injected intravenously with pentamidine isethionate (4 mg/kg in 0.9% physiological
583 saline) in the absence and presence of concomitant dosing with F68 (initial plasma concentration,
584 calculated by estimating plasma volume at 10% of body weight) at 0.025%. Each group had an n = 3.
585 Blood (<10 μl) was collected using a heparinized syringe at 1, 30, 120, 600 minutes post-injection and
586 plasma prepared. Both blood and plasma samples were snap frozen on dry ice and stored at -80°C
587 before analysis. After the last blood sample, the mice were perfused with sterile 0.9% physiological
588 saline (via the hepatic portal vein), the brains removed, weighed and snap frozen. Analysis of samples
589 was by a validated weak cation exchange solid phase extraction (WCX-SPE) approach performed by a
590 specialist contract research organization (Cyprotex). Briefly samples were diluted with water, WCX-
591 SPE sorbent was primed with MeOH and then water (to ensure phase was fully ionised). Samples
592 were then loaded onto sorbent and washed with pH7 buffer and MeOH. Pentamidine was then
593 washed off sorbent by eluting with a combination of MeOH/H_2O + 5% v/v formic acid. If necessary
594 samples were then evaporated to dryness and reconstituted in injection solvent. Samples were

595 analysed by UPLC-MS/MS as described above. LLOQ in plasma samples was 2 ng/ml and in brain
596 samples was 80 ng/ml.

597 Additional experiments revealed that intravenous administration of 10mg/kg pentamidine isethionate
598 plus or minus 0.5% F68 was toxic to the mice and the experiment was terminated.

599 **Data analysis.** All data are presented as means ±S.E.M and statistical analysis was carried out using
600 Sigma Stat software, version 12.0 (SPSS Science Software UK Ltd, Birmingham, UK).

601 **2.9 Trypanocidal activity *in vitro***

602

603 *In vitro* activity of drug formulations against *Trypanosoma brucei* blood stream form trypomastigotes
604 was determined *in vitro* using Alamar Blue (resazurin: Bio-Source, Camarillo, CA) as described by [52].
605 Prior to determination of the trypanocidal activity of Pluronic-pentamidine combinations, the IC_{50}
606 values of the Pluronic alone was established. Each Pluronic was tested in a 3-fold serial dilution in
607 triplicate and in three separate experiments (n=3). The diluent was HMI-9 media (Invitrogen, UK).
608 Blood stream form *T. b. brucei* (strain S427) trypomastigotes, cultured in modified HMI-9 media
609 supplemented with 10% v/v heat-inactivated foetal calf serum, (hi-FCS, Gibco, Life Technologies,
610 UK), were incubated (37°C; 5% CO_2) at a density of 2 x 10^4/ml in the presence of pentamidine alone or
611 pentamidine-Pluronic formulations for 66h. Resazurin (20 µl 0.49mM in PBS) solution was then added
612 to each well and incubation continued for 6 hours. After incubation, samples were removed and
613 fluorescence was measured using excitation 530nm and emission 590nm on a Spectramax M3 plate
614 reader (Molecular Devices, USA). IC_{50} values were determined (where appropriate) using GraphPad
615 Prism.

616

617 # 3. Results

618 ## 3.1 Evaluation of potential neurotoxicity of pentamidine

619 ***3.1a Literature review.*** We conducted a brief review of the literature to assess the potential
620 neurotoxicity of pentamidine. Information was considered relevant to the NanoHAT project if it
621 described an activity that could be detected in a simple profiling screen, rather than secondary
622 readouts (e.g. hERG-mediated, downstream effects on cardiomyocyte [Ca^{2+}]i). Table 2 lists the known
623 pharmacology and approximate affinities of the interaction that have been reported for this
624 compound.

625 As the trypanocidal activity of pentamidine occurs at around 10 nM *in vitro*[53], we considered that
626 any affinity greater than 1 µM (i.e. more than 100-fold greater than the trypanocidal concentration)
627 was unlikely to be relevant.

628

629 **Table 2. Reported Pharmacology of Pentamidine *in vitro.***

Property	Affinity (µM)	Comments	Reference
Trypanocidal	0.01	Time-dependent	[53]
$Imidazoline_2$ receptor	0.014	3H-idazoxan binding	[54]
Potassium channel expression/function	0.17	K(v)11.1(hERG) expression, K(IR)2.1 block	[55]; [56]
NMDA (Ionotropic) glutamate receptor	0.2	Voltage dependent	[57]
Human anti-platelet	1.1	Inhibits fibrinogen binding to GP11b/IIIa	[58]
Rat NMDA receptor	1.8	Rat brain membrane 3H-dizocilpine binding	[59]
PRL phosphatases	3	Oncology target	[60]
Delta2glutamate receptor	5	Voltage independent	[57]
Calmodulin antagonist	30	Inhibits nNO synthase	[61]

		in vitro	
Acid sensing ion channels (ASIC)	38	Potency 1b>3>2a>or=1a	[62]
Serine proteases	4000		[63]

630

631 There are 3 major target families for which pentamidine has significant affinity (<20 fold above
632 trypanocidal range) that were of concern: the imidazoline$_2$ receptor (responsible for effects on central
633 blood pressure control and pancreatic beta cells); inward rectifying (IR) potassium channels
634 particularly blockade of Kir2.1 (this is more likely cardiac than CNS-relevant) and NMDA glutamate
635 receptors.

636

637 ***3.1b*** **A neurological profiling screen**

638 A wide ligand profiling screen was carried out against 40 CNS targets (Perkin Elmer customised CNS
639 screening; listed in Table S1), testing at a single concentration of 10 μM (1000-times the trypanocidal
640 concentration), with follow up concentration-response curves in any assay where there was greater
641 than 70% inhibition. Pentamidine was inactive at 29 out of 40 CNS targets (including 5 glutamate
642 receptor binding sites) at 10 μM, and was re-tested against the remaining targets at a range of
643 concentrations to generate an inhibitory constant, K_i. These results, together with the calculated
644 relative selectivity values compared with trypanocidal affinity, are listed in Table 3.

645

646 **Table 3. K_i Values for Pentamidine Determined for Selected CNS targets.**

Target	K_i (μM)	Relative to trypanocidal activity
Trypanocidal Activity	0.01	1.0
Imidazoline 1_2	0.001	0.1
Monoamine oxidase B	0.181	18
Monoamine oxidase A	0.217	22
Adrenergic alpha1	0.273	27

Muscarinic (central)	0.281	28
Histamine H2	7.21	721
Opioid	1.41	141
DA transporter	2.11	211
Adrenergicalpha2	10	1000 Estimate from single-point screen
Adrenergic β	10	1000 Estimate from single-point screen
5HT transporter	10	1000 Estimate from single-point screen

Selectivity screening of pentamidine identified 5 targets (imidazoline I_2 receptor; monoamine oxidase A and B; adrenergic α_1 receptor; muscarinic receptor) for which it has significant affinity, and which should be monitored as we progressed through the screening cascade. In particular, pentamidine's high affinity for the imidazoline receptor may explain the cardiovascular adverse events associated with this drug. The project team considered that remaining targets were of minor concern, as the adverse events of drugs targeting the adrenergic monoamine oxidase and muscarinic systems are reasonably well described. The relatively low affinity of pentamidine for the remaining targets (histamine H_2 receptor; opioid receptor; adrenergic α_2, β receptors; 5HT transporter) indicated that the drug was unlikely to have significant effects until plasma/brain levels exceeded ~ 100-fold the trypanocidal concentration.

***3.1c* Ion channel screen**

We carried out ion channel screening at Chantest in order to investigate the potential potassium (K(IR)2.1) blocking liability reported by de Boer et al., (2010) (Table 2). Pentamidine isethionate salt was evaluated at 0.001, 0.01, 0.1, 1 and 10 µM (Table S2). The IC_{50} value for pentamidine isethionate salt could not be calculated as the highest tested concentration resulted in hKir2.1 inhibition less than 50% (i.e. 12.3±1.3%). The IC_{50} is estimated to be greater than 10 µM. The positive control (100 µM barium) confirms the sensitivity of the test system to ion channel inhibition.

667 **3.2 Formulation Development**

668 As this was a milestone driven project an iterative, dynamic approach was utilized to select the lead
669 formulation to take forward as quickly as possible in the screening cascade (Fig 1), hence not all
670 Pluronic formulations were assessed with each of the methods.

671

672 ***3.2a Phase Behaviour***

673 L61 phase diagrams were evaluated by visual inspection from 20°C to 50°C for L61 alone and in
674 mixtures with P105 and/or F68 in water and saline solutions. L61 presents a cloud point around 24°C
675 [64]and F68 does not improve its solubility, while P105 does to some extent (Tables S3 and S4).

676

677 ***3.2b. Critical micelle concentration (CMC) by fluorescence spectroscopy***

678 CMC were measured for individual Pluronic and mixtures of F68, P85, P105 and L61 at 20°C and 37°C,
679 both in aqueous and saline (0.9 wt%) solutions, using the intensity of pyrene fluorescence emissions
680 (Table 4; Fig S2). Mixtures of two Pluronics in both aqueous (aq) and saline (sal) mediums were
681 prepared in either a fixed mass ratio of 1:1 or with the addition of 0.01% w/v L61 and the CMC
682 determined. All CMC curves show two inflection points, a feature widely reported in the literature;
683 the first corresponds to the onset of aggregation and was chosen as the CMC (Fig S2; Table 4), giving
684 the following values in saline solution at 37°C (g/L): $P85_{sal}$=0.042±0.018; $F68_{sal}$=0.048±0.012 and
685 $P105_{sal}$=0.069±0.020. Overall, these CMC values are fairly similar and do not allow a prioritisation
686 based on CMC alone. The CMC of F68 and P85 mixtures (1:1 mass ratio) is about double the CMC ,
687 when expressed in total Pluronic mass, of the individual polymers suggesting the absence of mixed
688 micelles in these mixtures. Small amounts of L61 (0.01%w/v) does not affect the CMC of F68 or P85 or
689 P105 under the conditions tested.

690

691 **Table 4. CMC Values of Pluronic Dissolved in Pure Water (aq) or Saline (sal) at 20°C and 37°C**
692 **Determined Using Pyrene Fluorescence Intensity. Values Mean ± S.D. Saline (0.9 wt%).**
693

Temperature Sample	20°C g/L	37°C g/L
	CMC	**CMC**
$P85_{aq}$ $P85_{sal}$	0.3197±0.0067 0.1460±0.0311	0.0432±0.0075 0.0424±0.0178
$F68_{aq}$ $F68_{sal}$	0.2737±0.0311 0.2730±0.0029	0.0606±0.0045 0.0476±0.0119
$P105_{aq}$ $P105_{sal}$	0.2429±0.0140 0.1905±0.0093	0.0730±0.0136 0.0686±0.0191
$L61_{aq}$ $L61_{sal}$	0.0299±0.0320 0.0240±0.0236	n.a. n.a.
Fixed ratio 1:1 mixtures		
$P85+F68_{aq}$ $P85+F68_{sal}$	0.7415±0.0000 0.6777±0.0000	0.0951±0.0000 0.0993±0.0000
$P85+L61_{aq}$ $P85+L61_{sal}$	0.2678±0.0000 0.3024±0.0000	n.a. n.a.
Sample + L61 (0.01w/v%)		
$P85_{aq}$ $P85_{sal}$	0.1135±0.0035 0.2836±0.1278	0.0508±0.0264 0.0734±0.0316
$F68_{aq}$ $F68_{sal}$	0.2010±0.0042 0.2060±0.0283	0.0510±0.0177 0.0430±0.0000
$P105_{aq}$ $P105_{sal}$	0.2421±0.0298 0.1938±0.0139	0.0705±0.0237 0.0833±0.0475

694

695 ***3.2c Stability of the formulations***:

696 Pentamidine stability in solution was followed by NMR. Pentamidine and pentamidine/Pluronic
697 solutions prepared in D_2O were kept in amber NMR tubes at 37°C. Spectra were measured at days 0, 1
698 and 7. As a control, pentamidine in D_2O was left at 4°C and measured at day 0 and 7. NMR data
699 showed no significant change on peak position or peak intensity when compared to day 0

700 measurements or to control samples, confirming no thermal degradation of pentamidine after 7 days

701 at 37°C.

702

703 ***3.3d Partition***

704 Partition of PTI in the micelles was measured by fluorescence spectroscopy for P105 and F68.

705 Pentamidine has a slightly larger partition coefficient in F68 than in P105 (Table 5). Measurements in

706 mixtures (F68/L61, P105/L61 and F68/P105, 1:1 mass ratio in all cases) do not significantly change the

707 partition coefficient (data not shown).

708 The values of Log P obtained in saline and aqueous solutions are rather similar, suggesting that

709 pentamidine partition is not sensitive to the saline levels used here.

710 The effect of temperature is quite weak (Table 5), and does not follow the same trend with the two

711 Pluronic studied: values of LogP for P105 are lower at 20°C than at 37°C (but still very close); instead,

712 for F68 the partition of PTI decreases slightly at higher temperature.

713 At biologically relevant concentrations, 0.5 wt% Pluronics and 1.0×10^{-6} M PTI, extrapolation of the Log

714 P data suggest that ca. 0.1 PTI molecules would be incorporated in one P105 micelle, and 0.01 PTI

715 molecules in one F68 micelle. At the concentrations used for SANS (5 wt% Pluronic and 1 wt% PTI),

716 extrapolating these numbers give 166 PTI molecules in the micellar core per P105 micelle and 15 for

717 F68 micelle.

718 The relative low values of log P for PTI/Pluronic system (for comparison log P for pyrene/Pluronics is

719 ca. 2.5 and 3.5 for F68 and P105, respectively [11]), is not surprising given the high water solubility of

720 pentamidine, and helps to explain the drug release profile for PTI / Pluronics systems discussed next.

721 Overall, this means that Pluronic have a limited capacity to interact with pentamidine and prolong its

722 circulation.

723

724 **Table 5. The fraction of pentamidine incorporated into the Pluronic micelle expressed as a**
725 **partitioning coefficient, P. The Pluronic was dissolved in pure water (aqueous) or saline (saline) at**
726 **20°C and 37°C. (Also see Fig S3).**

727

Pluronic	Solvent	Temperature °C	Log P
P105	saline	20	1.06
		37	1.15
P105	water	20	0.99
		37	1.09
F68	saline	20	1.67
		37	1.47
F68	water	20	1.67
		37	1.46

728

729 ***e. Drug release***

730 Solutions of 10 mM pentamidine or 10 mM pentamidine plus 1 % F68 or 1% P105 were loaded in
731 dialysis cells and the amount of pentamidine eluting from the cells into water at 37°C were measured
732 over time (Fig S4). Both reaction type and reaction constant, for PTI alone and PTI/Pluronic were in a
733 similar range. ca. 0.5 (Fickian diffusion) for reaction type and ca 0.3 for reaction constant. No
734 significant difference was observed between PTI/Pluronics and PTI/water systems. Thus in the
735 conditions tested, pentamidine release seems to be dominated by diffusion and Pluronic micelles
736 were not a barrier for drug release.

737

738 ***f. Aggregation number and Micellar size:***

739 Pluronic micelles can be reasonably described as a compact core formed by a dry PPO block
740 surrounded by a highly hydrated shell formed by the two PEO blocks[65][66]. The core-shell model
741 was thus used to provide a more detailed characterisation of the morphology of the Pluronic
742 micelles in D_2O and how it is affected by the presence of PTI, using input values for the core radius
743 and shell thickness were based on hydrodynamic radius values obtained by DLS (Table 6). A term
744 to compensate for polydispersity was included for both Pluronics, as well as a structure factor
745 ($S(q)$), corresponding to a hard sphere model, in order to account for intermicellar interactions. A

746 summary of the main parameters obtained from the analysis of the data (Fig S5) is present in

747 Table 7.

748

749 **Table 6. Stokes Radii of P105, P85 and F68 Micelles Obtained from DLS (1% w/w, 37°C).**

Pluronic$_{(aq)}$	**Radius (nm)**	**Pluronic$_{(saline)}$**	**Radius (nm)**
F68	2.8	F68	2.5
P85	6.6	P85	6.5
P105	8.1	P105	8.0
[PTI]= 10^{-6} M		[PTI]= 10^{-6} M	
F68	2.8	F68	2.6
P85	6.6	P85	7.8
P105	7.7	P105	6.7
PTI - 1:3 mass ratio		PTI - 1:3 mass ratio	
F68	2.3	F68	3.1
P85	6.8	P85	6.5
P105	8.1	P105	8.0

750

751 **Table 7. Geometric parameters from model-fitting of the SANS Pluronic data at 37°C,**
752 **including core and shell micellar sizes, fraction of solvent in the corona (χ_{solv}) and**
753 **aggregation number (N_{agg}). (Also see Fig S5).**

Sample	**Core radius (Å)**	**Shell thickness (Å)**	**Total radius (Å)**	**χ_{solv}**	**N_{agg}**
F68 5%	15.4	36.5	52.0	0.99	2.37
F68 5%/ PTI 1%	15.1	34.7	49.8	0.98	2.25
F68 5%/ PTI 3%	15.5	33.9	49.4	0.99	2.38
P85 5%	42.9	31.4	74.3	0.95	35.4
P85 5%/ PTI 1%	41.5	30.5	72.0	0.95	32.4
P85 5%/ PTI 3%	41.0	30.5	71.5	0.99	31.6

754

755 A direct comparison of F68 and P85 micelles in D_2O shows that both have similar shell thickness, with
756 F68 showing values slightly larger, 36.5 Å vs 31.4 Å, respectively. It is worth noting that F68 EO blocks
757 have on average 76.4 EO units while P85 blocks are only 26.1 units long. The core of F68 micelles are
758 significantly smaller than P85 micelles, 15.4 vs 42.9 Å. In terms of PO content, the F68 PO block is 29
759 units long while P85 is 40 units long. Overall, P85 micelles are larger than F68 micelles, 74.3 vs 52.0 Å,
760 respectively.
761
762 The simulation work agrees well with these experimental results. The average aggregation number
763 per micelle (N_{agg}) and the average number of micelles (N_{mic}) were calculated once the systems had
764 equilibrated have been measured. Fig 2 shows plots of N_{agg} and N_{mic} as a function of Pluronic
765 concentration for both the F68 and P105 Pluronics. We carried out simulations over a range of
766 Pluronic concentrations that span the CAC and the CMC values observed experimentally to validate
767 the models (at least qualitatively). From Fig 2, one can see that in both systems, once we have passed
768 the CAC the number of micelles remains more or less constant but they continue to grow in size as the
769 concentration increases until we reach the CMC at which point the size of the micelles more or less
770 plateaus. Also, when comparing the behavior of the F68 and P105 Pluronics, we found that the P105
771 Pluronics form larger aggregates when near the CMC as compared to that for the F68 Pluronics, and
772 therefore fewer micelles. Note, we have also simulated mixtures of F68 and L61 Pluronics, and the
773 results of those systems are presented in Fig S6.
774
775 **Fig 2. The average number of Pluronic molecules found in a micelle (N_{agg}) and the number of**
776 **micelles in our system (after they have equilibrated) (N_{mic}) as a function of the concentration**
777 **of the Pluronics in the system for both the F68 (left) and P105 (right) Pluronics**. Additionally,
778 we have compared the findings from the simulations with the identified values (dashed lines) of
779 the CAC and CMC from the experimental systems.
780
781 In the presence of 1% PTI, a small reduction in size was observed for both Pluronics, ca. 2 Å in both
782 cases. The increase to 3% PTI does not cause further changes.

783 The coronas were highly hydrated, as reported for these polymers [67][68]. F68 micelles were more
784 hydrated than P85: for each EO unit in the shell, there were are 17 D_2O molecules in a F68 micelle but
785 only 3.4 in a P85 micelle.
786 The addition of pentamidine leads to a subtle, but perceptible, reduction of the number of water
787 molecules in the F68 micelle shell. For P85, no measurable changes were observed.
788
789 **3.3 Peripheral Toxicity**
790 Pluronic concentrations used in the biological assays were based on the CMC measurements.
791 Peripheral toxicity of the individual polymers was assessed. L61 was not studied at this stage due to
792 its limited solubility.
793
794 **a. Haemolysis assay**
795 All the Pluronics (P85, F68 and P105) at each of the tested concentrations (0.01%, 0.1%, 0.25%, 1% or
796 5%) and both the negative controls (0.05% DMSO or 0.9% saline) did not cause any haemolysis (0%) of
797 the human cells. In contrast the positive control, 10% Triton X-100, caused haemolysis (***$p<0.001$
798 compared to the negative controls).
799
800 **b. Permeability assay (MDCK-MDR) to assess membrane integrity**
801 [^{14}C(U)]sucrose is an inert, polar molecule which normally does not cross cell membranes, but may
802 cross between cells through the paracellular cleft. Significant differences in [^{14}C(U)]sucrose P_{app} values
803 existed in the presence of all tested concentrations of P85, and 0.5% and 0.01% P105 compared to
804 [^{14}C(U)]sucrose P_{app} in the absence of Pluronic (Fig S7) indicating loss of monolayer integrity. No
805 tested concentration of F68 significantly affected the radiolabelled sucrose P_{app} values.
806
807 **c. Effect of Pluronic on insulin secretion and beta-cell viability**

808 Exposure of MIN6 β-cells to 1 and 100μM pentamidine for 24 hours caused a concentration-
809 dependent inhibition of acute insulin secretion in response to the cyclic AMP elevating agents
810 forskolin and IBMX (Fig 3). Surprisingly, P85 and 105 were significantly more effective than
811 pentamidine in inhibiting insulin secretion in response to forskolin/IBMX, such that insulin release was
812 fully inhibited by these Pluronics in the absence of pentamidine at all concentrations tested (0.01-0.5%
813 w/v) (Fig 3A-D). Low concentrations of F68 (0.01 and 0.025% w/v) generated similar inhibitory effects
814 on insulin secretion as unformulated pentamidine (Fig 3A-B) and increased toxicity was observed with
815 higher concentrations of F68 (Fig 3C-D).

816

817 **Fig 3. The effect of Pluronic and pentamidine in DMEM on insulin secretion from MIN6 β-cells**
818 **expressed as a percentage of control.** Control values were obtained from DMEM supplemented with
819 2mM glucose. (A-D) P85 and P105 induced a strong suppression of insulin secretion from MIN6 β-cells
820 even at low concentrations. (C-D) F68 only induced insulin secretion suppression at concentrations
821 ≥0.1% w/v.

822

823 Trypan blue staining indicated that the MIN6 β-cells were able to tolerate pentamidine concentrations
824 of 1 and 10 μM, but 100 μM pentamidine, which induced maximal inhibition of insulin secretion, was
825 accompanied by a large number of cells taking up Trypan blue (Fig S8 and S9). These micrographs are
826 indicative of the suppression of insulin secretion by pentamidine being associated with marked
827 reductions in β-cell viability, but the plasma membrane was largely intact as there was no leakage of
828 insulin, a 5.5 kDa peptide, from the cell interior. The combination of 100 μM pentamidine with 0.5%
829 w/v F68, which caused maximal suppression of insulin release (Fig 3), led to the highest proportion of
830 cells that showed Trypan blue staining.

831

832 **3.4 *Trypanocidal activity in vitro***

833 *The In vitro* activity of Pluronic drug formulations alone against *T. b. brucei* blood stream form
834 trypomastigotes was determined showing low trypanocidal activity of F68 compared to high activity of
835 P85 and P105 (Table 8).

Table 8. The Inhibitory Concentration (IC_{50}) required to reduce number of bsf trypomastigotes by 50%. Pluronic were tested at 12 serial dilutions in triplicate and repeated in 3 separate experiments (n=3) to produce IC_{50} values.

w/v %	F68	F68/0.01% L61	P85	P105
IC_{50}	0.48%	0.46%	0.00021%	0.00084%
95% CI	0.38 - 1.35	0.027 - 0.94	0.00056 - 0.0014	0.00070 - 0.0012

In further studies the anti-trypanosomal activity of combinations of F68 and pentamidine were assessed (Table 9). The IC_{50} (± 95% CI) values of pentamidine were 2.11×10^{-5} ± (1.79×10^{-5} – 2.50×10^{-5}) µM alone, 6.36×10^{-6} (± 4.43×10^{-6} – 9.12×10^{-6}) µM with 0.01% F68 and 3.25×10^{-6} ± (3.13×10^{-7} – 3.38×10^{-5}) µM with 0.001% F68.

Table 9. The % of bsf trypomastigotes inhibited by pentamidine/pluronic combinations. The combination formulation was tested in triplicate and repeated in 3 separate experiments (n=3).

	Pentamidine (µM)					
	1	**0.3**	**0.000152**	**5.1×10^{-5}**	**1.7×10^{-5}**	**5.7×10^{-6}**
F68 (w/v %)						
0.5%	99.5%	98.6%	98.6%	98.3%	98.3%	99.2%
0.1%	98.5%	97.7%	97.1%	97.1%	97.3%	97.7%
0.025%	98.3%	97.5%	97.0%	96.9%	97.0%	90.6%
0.01%	98.4%	97.6%	96.4%	95.1%	82.8%	3.4%
0.001%	98.3%	97.4%	96.4%	91.9%	73.1%	1.8%
0%	98.3%	97.4%	92.7%	65.3%	35.0%	4.1%

To determine if the addition of Pluronic to pentamidine had an additive effect on the trypanocidal activity of pentamidine, it was decided that work should focus on F68 rather than the other Pluronics, as both P85 and P105 caused an inhibitory effect on insulin secretion. Although IC_{50} values could only

853 be determined for two combinations, in part due to the high starting concentration of pentamidine
854 used, a limited interaction between Pluronic F68 and pentamidine was observed at the lowest F68
855 concentrations (Table 9 boxes shaded in red), suggesting that the addition of Pluronic had an additive
856 effect on the trypanocidal activity.
857

858 **3.5 Blood-brain barrier: *In vitro* permeability assays**

859 We examined the ability of different pentamidine-Pluronic formulations to cross the BBB using the
860 MDR1-MDCK cell line. Two analytical methods were applied: one detected pentamidine isethionate
861 using UPLC-MS/MS (Table S5) and the other detected radiolabelled pentamidine using liquid
862 scintillation counting (Table 10).

863 The ability of pentamidine isethionate to cross the MDR1-MDCK cell monolayers in the apical (luminal)
864 to basolateral (abluminal) direction was limited as the concentration of pentamidine isethionate in the
865 basolateral chamber were below the limits of UPLC-MS/MS detection, even when the pentamidine
866 isethionate concentration was increased to 20 μM (data not shown). The lower limit of quantification
867 (LLQ) for UPLC-MS/MS method was ≤ 7.8 nM which is equivalent to <0.039% of the dose in the donor
868 (apical) chamber. These results would suggest that pentamidine is a 'CNS negative' drug. The mass
869 balance (% recovery) results suggest that up to 25% may have been trapped either in the endothelial
870 cells or by non-specific binding to the plastic plate or the polycarbonate membrane and this may
871 contribute to the reduced recovery. It is important to note that the two amine groups of pentamidine
872 are ionized at physiological pH (pKa is 11.4) and are likely to react with static charges on the surface of
873 plastics. Interestingly the presence of Pluronic increased the mass balance results by 10-20%. In
874 contrast the movement of pentamidine isethionate (20μM) across the monolayer in the basal to apical
875 direction was measurable, the calculated P_{app} being 0.418 x 10^{-6} cms^{-1}. Taken together with the
876 absence of a detectable movement of pentamidine isethionate in the apical to basolateral direction
877 these data would indicate the presence of an efflux mechanism for this molecule, likely MDR1. The

878 presence of Pluronics (F68, P105 or P85 at concentrations of 0.01%, 0.1% or 0.5%) did not affect the
879 distribution of pentamidine isethionate across the monolayer in either direction.

880 MDR1-MDCK permeability assay experiments were also performed using radiolabelled pentamidine
881 and liquid scintillation counting. The rate of transport of [^{3}H(G)]pentamidine (9 nM) across MDR1-
882 MDCK monolayer was examined and in contrast to the results achieved with the pentamidine
883 isethionate was measurable in both directions (Table S5). In these experiments the highest
884 concentrations of P85 (0.5%) and P105 (0.5%) affected the integrity of the cell monolayer and the
885 Papp for [^{14}C(U)]sucrose was increased to 4.8 and 4.3 x 10^{-6} cm/s respectively. The [^{14}C(U)]sucrose P_{app}
886 for all other experiments was 1.61±0.15 x 10^{-6} cm/s. The presence of the Pluronics (F68, P105 or P85)
887 at concentrations of 0.01% and 0.1% did not significantly increase the distribution of
888 [^{3}H(G)]pentamidine across the MDR1-MDCK monolayer measured over 60 minutes confirming the
889 results obtained using pentamidine isethionate and the UPLC-MS/MS detection method.

890 In conclusion, our target formulation characteristics of at least a 2-fold increase in pentamidine /
891 pentamidine isethionate movement across the monolayer, compared with unformulated pentamidine,
892 was not observed using these *in vitro* models of BBB permeability.

893 **Table 10. The Effect of P85, F68 and P105 on the Apparent Permeability of [^{3}H(G)]pentamidine (9**
894 **nM) MDR1-MDCK Cell Monolayers in the Apical to Basolateral Direction and the Basolateral to**
895 **Apical Direction. The percentage recovery of pentamidine is also shown. All the data has been**
896 **corrected for extracellular space by subtracting [^{14}C(U)]sucrose (5.5 μM) P_{app} values which ranged**
897 **from 0.89 to 2.00 x 10^{-6} cm/s. Each value represents three replicates for each n and n =3. n.d. = not**
898 **determined as integrity of the barrier compromised.**

[^{3}H(G)]Pentamidine (9 nM)	**Pluronic Concentration (%)**	**P_{app} A2B (10^{-6} cm/s)**	**P_{app} B2A (10^{-6} cm/s)**	**A2B (%)**	**B2A (%)**
		Mean±SEM	**Mean±SEM**	**Mass balance**	**Mass balance**
	0	0.678±0.025	0.776±0.062	84	85
	0.01% P85	0.310±0.142	0.431±0.161	86	87
	0.1% P85	0.561±0.0.172	0.227±0.081	89	89

	0.5% P85	n.d.	n.d.	90	90
	0.01% P105	0.577±0.0710	0.818±0.086	86	89
	0.1% P105	0.898±0.161	0.776±0.054	89	88
	0.5% P105	n.d.	n.d.	91	91
	0.01% F68	0.200±0.115	0.106±0.061	95	83
	0.1% F68	0.221±0.067	0.033±0.019	98	87
	0.5% F68	0	0	98	84

899

900 **3.6: Blood-brain barrier *In situ* brain perfusion**

901 ***3.6a* PLURONIC P85**

902 Co-formulation of 15.7 nM [^{3}H(G)]pentamidine with Pluronic P85 did not significantly increase
903 [^{3}H(G)]pentamidine accumulation in any of the brain regions examined (Table S6).

904 In fact, overall there was a decrease in the [^{14}C(U)]sucrose-corrected uptake of [^{3}H(G)]pentamidine
905 with P85 at 0.01% ($p<0.001$) and at 0.1% ($p<0.01$) (Two-Way ANOVA), but these decreases were not
906 statistically significant when individual brain regions were examined using Bonferroni's pairwise
907 comparisons.

908 Table S6 shows the results of capillary depletion analysis of the brain tissue after 10 minutes of
909 perfusion in the presence or absence of the Pluronic, P85. [^{3}H(G)]pentamidine accumulated in the
910 capillary endothelial cells (pellet) of control mice while less than 2% of the plasma concentration
911 crossed the basolateral membrane to reach the parenchyma (supernatant). These results are in good
912 agreement with our previously published data[49]. There appeared to be an overall reduction in this
913 accumulation of [^{3}H(G)]pentamidine into the endothelial cells and consequently a reduction in the
914 parenchyma when [^{3}H(G)]pentamidine was co-formulated with 0.01% and 0.1% P85, but the reduction
915 did not attain statistical significance (Two-Way ANOVA with Bonferroni's pairwise comparisons).

916 Whilst there appeared to be an overall inhibitory effect of Pluronic on the transport of
917 [^{3}H(G)]pentamidine across the BBB, there was a significant, 3-fold increase in the uptake of

918 [^{3}H(G)]pentamidine into the pituitary gland after 10 minutes of perfusion with 0.1% and 0.5% P85
919 ($p<0.05$ at both concentrations; Two-way ANOVA with Bonferroni's pairwise comparisons). This
920 enhanced uptake of pentamidine appeared to be associated with an approximate 2-fold increase in
921 accumulation of [^{14}C(U)]sucrose from 20.5±3.9% ([^{14}C(U)]sucrose alone) to 35.0±5.5% (+0.01%P85),
922 43.0±4.0% (+0.1% P85) and 34.3±7.9% (+0.5% P85). A similar effect was observed in the choroid
923 plexus sampled from a few individual mice that were perfused with pentamidine co-formulated with
924 P85 at concentrations above the CMC. This resulted in a 2-fold increase in the mean uptake of
925 [^{3}H(G)]pentamidine which was not statistically significant. P85 did not affect accumulation of
926 [^{3}H(G)]pentamidine or [^{14}C(U)]sucrose by the pineal gland.

927 **3.6b PLURONIC P105**

928 An overall decrease in the [^{14}C(U)]sucrose-corrected uptake of [^{3}H(G)]pentamidine into brain
929 parenchyma was observed when 15.7nM [^{3}H(G)]pentamidine was co-formulated with 0.1% ($p<0.001$)
930 and 0.5% ($p<0.001$) P105, as shown in Table S7, but (like P85) these data did not reach statistical
931 significance in any of the individual regions sampled (Two-Way ANOVA with Bonferroni's pairwise
932 comparisons).

933 In contrast, there was a 33% increase in the [^{14}C(U)]sucrose-corrected uptake of [^{3}H(G)]pentamidine
934 into the endothelial cell pellet when it was co-formulated with 0.1% P105 ($p=0.027$; Two- way ANOVA
935 with Bonferroni's pairwise comparisons). This increase was apparent in only 3 out of 6 mice, and was
936 associated with penetration of the brain tissue by the vascular space marker [^{14}C(U)]sucrose, perhaps
937 indicating an increase in the permeability of the apical/luminal endothelial cell membrane.

938 No significant differences were observed in the uptake of either the vascular space marker
939 [^{14}C(U)]sucrose or [^{3}H(G)]pentamidine into the pineal gland, choroid plexus or pituitary gland after 10
940 minutes of perfusion with [^{3}H(G)]pentamidine co-formulated with P105 as shown in Table S7 ($p>0.05$

941 for each Pluronic concentration and circumventricular organ; Two-way ANOVA with Bonferroni's
942 pairwise comparisons).

943 **3.6c PLURONIC F68**

944 **10 minute perfusions**

945 Co-formulation of [^{3}H(G)]pentamidine with F68 resulted in an overall decrease in accumulation of
946 [^{3}H(G)]pentamidine into brain parenchyma after 10 minutes of perfusion (p=0.002 for 0.1% and p=0.03
947 for 0.5% respectively; Two-way ANOVA with Bonferroni's pairwise comparisons) (Table S8). A
948 decrease in vascular space as measured by accumulation of [^{14}C(U)]sucrose was also measured when
949 0.01 or 0.1% F68 (but not 0.5%) was present in the artificial plasma (p=0.042 for 0.01% and p=0.004
950 for 0.1% respectively; Two-way ANOVA with Bonferroni's pairwise comparisons) (Table S9).

951 F68 did appear to increase accumulation of [^{3}H(G)]pentamidine into the endothelial cell pellet at
952 concentrations of 0.01% and 0.1%, but these results did not attain significance. This increase in
953 [^{3}H(G)]pentamidine, did not appear to be associated with a concomitant increase in uptake of
954 [^{14}C(U)]sucrose (p>0.05) and might have been due, at least in part, to a small decrease in the amount
955 of drug crossing the basolateral membrane to enter the brain parenchyma, as indicated by a marginal
956 reduction of [^{3}H(G)]pentamidine in the supernatant (Table S8).

957 Co-formulation of [^{3}H(G)]pentamidine with 0.5% F68 resulted in a 2-fold increase in uptake into the
958 pituitary gland after 10 minutes of perfusion (p=0.017; 1-way ANOVA with Bonferroni's pairwise
959 comparisons). A similar, but not statistically significant increase was observed in uptake of
960 [^{14}C(U)]sucrose into this organ over the same time period.

961 **30 minute perfusion**

962 Accumulation of [^{14}C(U)]sucrose measured in brain parenchyma, as a percentage of concentration in
963 the artificial plasma ($R_{TISSUE/PLASMA}$%), ranged from 1.3% in the hippocampus to 4.3% in the pons after 30

964 minutes of perfusion. These values are almost identical to our previously published data for BALB/c
965 male mice (1.6 and 4.5% respectively)[7]. Accumulation of [^{3}H(G)]pentamidine, when corrected for
966 vascular space ranged from 6.9% in the hippocampus to 15% and 10.9% in the more highly
967 vascularized regions of the hypothalamus and pons respectively. These values were slightly higher
968 than our previously published data (4.3% for hippocampus, 7.6% for hypothalamus and 8.2% for pons)
969 and might reflect changes in expression of transporters due to differences in environment/diet or
970 selective pressures during breeding.

971 Formulation of 15 nM [^{3}H(G)]pentamidine with 0.01% or 0.1% F68 did not affect [^{14}C(U)]sucrose brain
972 space (p=0.139 and 0.460 respectively; 2-way ANOVA with Bonferroni's post-tests). No significant
973 differences were observed in [^{3}H(G)]pentamidine accumulation at these concentrations (p=0.120 and
974 1.000 respectively; 2-way ANOVA with Bonferroni's post-tests). Similarly, F68 had no significant effect
975 on [^{14}C(U)]sucrose or [^{3}H(G)]pentamidine accumulation in the capillary depletion samples after 30
976 minutes of perfusion (p>0.05 for each concentration tested for each isotope; 2-Way ANOVA) nor in
977 the circumventricular organs (p>0.05 for each concentration tested for each isotope; 2-Way ANOVA).

978 There was an approximate 2-fold increase in accumulation of both [^{3}H(G)]pentamidine and the
979 vascular space marker [^{14}C(U)]sucrose in the brain parenchyma of mice that were perfused with
980 formulations containing 0.5% F68, (p=0.003 and p <0. 001 respectively; 2-way ANOVA with
981 Bonferroni's post-tests), as shown in Table S10A and S10B. Visible signs of damage to the BBB
982 including permeation and staining with Evans blue (MW 961), were also observed in some mice. The
983 results from the capillary depletion analysis after 30 minutes of perfusion would also appear to reflect
984 damage to both the apical and basolateral endothelial cell membranes, with a tendency for increased
985 permeation of [^{14}C(U)]sucrose into the brain parenchyma, as demonstrated by a small, though not
986 statistically significant rise in this isotope being detected in the supernatant (Table S10).

987 Co-formulation of [^{3}H(G)]pentamidine and [^{14}C(U)]sucrose with 0.5% F68 resulted in an increase into
988 the pituitary gland and the choroid plexus when the perfusion time was extended to 30 minutes,
989 although these results were not statistically significant.

990 ***3.7 In vivo* pharmacokinetic experiments with pentamidine isethionate or [^{3}H(G)]pentamidine.**

991 F68 at the 0.025% does not change the accumulation of pentamidine isethionate in the plasma, brain
992 parenchyma or blood in the mouse up to 10 hours post-dosing (Fig 4). There might be a late-onset
993 increase in brain concentrations in the pentamidine alone group, but as the standard deviations for
994 this group at this time-point are large this is unlikely to be significant.

995 **Fig 4. The effect of Pluronic F68 on pentamidine concentrations in mouse plasma, blood and brain**
996 **after an intravenous dose**. Each point represents an n of 3. 4mg/kg pentamidine ± 0.025% F68 i.v.
997 Values ± SD.
998
999 Table 11 shows the mean plasma and CSF (corrected for blood/sucrose contamination) concentrations
1000 for [^{3}H(G)]pentamidine and/or its metabolites, measured at 2 hours after intra-venous injection. No
1001 significant differences were observed when [^{3}H(G)]pentamidine was co-formulated with either 0.025%
1002 or 0.5% F68 ($p > 0.05$ for plasma and CSF; One-way ANOVA). Similarly, no significant differences were
1003 observed in uptake of [^{3}H(G)]pentamidine or the vascular space marker [^{14}C(U)]sucrose, into the brain
1004 parenchyma, capillary depletion samples or the circumventricular organs when [^{3}H(G)]pentamidine
1005 was injected in the presence or absence of F68 ($p > 0.05$; 2-way ANOVA with Bonferroni's pairwise
1006 comparisons) as shown in Table 12.

1007 **Table 11. Concentration of [^{3}H(G)]pentamidine/metabolites in the plasma and**
1008 **CSF at 2 hours post-injection.**
1009

Group	mean concentration in plasma ng/ml (± SEM)	mean concentration in CSF pg/ml (± SEM)
control	0.343 (± 0.061)	2.669 (± 0.765)
0.025% F68	0.345 (± 0.013)	1.948 (± 0.826)
0.5% F68	0.356 (± 0.026)	3.592 (± 1.932)

1010

1011 **Table 12. Uptake of [^{3}H(G)]pentamidine into brain tissue (corrected for vascular space) at 2 hours**
1012 **post-injection. Data is presented as the tissue/plasma ratio (a) and converted into concentrations in**
1013 **ng/g of tissue (b).** A limitation of measuring pentamidine by scintillation counting is that any
1014 metabolites produced during the 2 hours that have retained the radiolabel, will be counted as
1015 [^{3}H(G)]pentamidine. These metabolites may have different transport characteristics and may or may
1016 not be active against trypanosomes.

(a)	**$R_{TISSUE/PLASMA}$% (mean±SEM)**		
Region	**Control (15.7 nM pentamidine) (n=6)**	**0.025% F68 + (15.7 nM pentamidine) (n=6)**	**0.5% F68 + (15.7 nM pentamidine) (n=5)**
Right brain	115.52 (± 12.46)	120.29 (± 17.14)	87.36 (± 20.36)
Left brain	152.29 (± 33.48)	111.85 (± 19.15)	106.10 (± 12.92)
Cerebellum	204.02 (± 35.28)	208.87 (± 28.81)	172.48 (± 30.34)
Midbrain	181.18 (± 45.30)	254.02 (± 35.48)	180.00 (± 32.83)
Homogenate	249.41 (± 35.59)	184.18 (± 35.22)	293.81 (± 122.95)
Supernatant	123.35 (± 28.45)	99.72 (± 9.02)	98.66 (± 9.47)
Pellet	479.72 (± 72.50)	310.63 (± 38.62)	536.52 (± 212.72)
Choroid plexus	24666.66 (± 4928)	19628.89 (± 4672)	20463.70 (± 1827)
Pituitary gland	15053.41 (± 3598)	11285.42 (± 2008)	15061.87 (± 5321)

1017

(b)	**Mean concentration (ng/g or ng/ml for the supernatant ±SEM)**		
Region	**Control (15.7 nM pentamidine) (n=6)**	**0.025% F68 (15.7 nM pentamidine) (n=6)**	**0.5% F68 + (15.7 nM pentamidine) (n=5)**
Right brain	0.363 (± 0.035)	0.417 (± 0.061)	0.302 (± 0.058)
Left brain	0.472 (± 0.084)	0.383 (± 0.063)	0.375 (± 0.048)
Cerebellum	0.607 (± 0.032)	0.719 (± 0.097)	0.591 (± 0.084)
Midbrain	0.494 (± 0.075)	0.866 (± 0.115)	0.614 (± 0.072)
Homogenate	0.820 (± 0.183)	0.643 (± 0.132)	0.988 (± 0.375)
Supernatant	0.363 (± 0.037)	0.345 (± 0.035)	0.351 (± 0.043)
Pellet	1.482 (± 0.151)	1.067 (± 0.125)	1.827 (± 0.662)
Choroid plexus	74.68 (± 11.48)	84.04 (± 5.78)	72.20 (± 7.60)
Pituitary gland	43.76 (± 3.82)	37.58 (± 6.54)	68.13 (± 15.05)

1018

1019 ## Discussion

1020 In this study we generated pentamidine/Pluronic® formulations and prioritised 18 formulations using
1021 a rational, iterative approach (Fig 1). The milestones were intended to ensure that the most
1022 appropriate formulations, on the basis of *in silico* and *in vitro* data, were taken forward to the *in vivo*
1023 pharmacokinetic studies and that the formulations with the greatest likelihood of success would be
1024 assessed for toxicity issues *in vivo* and tested in animal efficacy models of stage 1 and stage 2 HAT. An
1025 ideal formulation for injection should be equipped with characteristics that improved the stability and
1026 safety profile of pentamidine, enhanced therapeutic effect, and accelerated the absorbance of drugs.

1027 Since increasing the concentration of pentamidine in the brain may cause an intractable neurotoxicity
1028 and serious adverse events our starting point was a customised, wide ligand profiling screen carried
1029 out against 40 CNS targets (Tables 2 and S1). Five targets (imidazoline I_2 receptor; monoamine oxidase
1030 A and B; adrenergic α_1 receptor; muscarinic receptor) were identified to have significant affinity for
1031 pentamidine (Table 3). All but one of these (imidazoline I_2 receptor) had a 20-1000 fold lower affinity
1032 than the relative trypanocidal activity and did not generate major concern[59]. The activity against
1033 the imidazoline I_2 receptor may explain the cardiovascular adverse events with this drug. We were
1034 unable to reproduce the result of De Boer et al., 2010[55] in a recombinant human system indicating
1035 that pentamidine was without effect (at up to 10 μM) on the hKir2.1 potassium channel-induced
1036 inward rectifying current (Tables 2 and S2). Thus progression could continue through the screening
1037 cascade.

1038 For the Pluronics tested in this study (P85, P105, F68 and L61), phase behaviour [69][33] and cloud
1039 points [70] are well established. P85, P105 and F68 are soluble in water and saline solutions at both
1040 24°C and 37°C. L61 has a very low cloud point at 24°C. Pure L61 therefore has limitations as a
1041 formulation for drug delivery. Our phase diagrams revealed that F68, which is highly hydrated, is
1042 unable to improve the solubility of highly hydrophobic L61 to a great extent, so it was not possible to
1043 pursue a 1:1 mixture of L61:F68 in the assays (Table S3 and S4).

1044

1045 Using molecular dynamics (MD) simulations and physical techniques, we elucidated the structural
1046 properties of Pluronic P85, P105, F68 and L61 micelles, and were able to extract fundamental
1047 parameters required for biological evaluation of the formulations. For example, the CMC were
1048 measured for F68, P85 and P105 at 20°C and 37°C both in aqueous as well as saline (0.9 wt%)
1049 solutions. Several values for the CMC of Pluronics can be found in the literature [71][72][73][11][74].
1050 These values tend to vary widely, showing as much as one order of magnitude differences for the
1051 same Pluronic[75]. This has been attributed to several reasons: difference in molecular weight
1052 distribution between batches [76][74], presence of impurities such as diblocks[76][77] and differences
1053 inherent to the technique employed[78]. In addition, for some Pluronic systems, two critical
1054 concentrations are detected, both in surface tension and spectroscopic experiments [76][72]. This
1055 behaviour has been ascribed to formation of premicellar aggregates occurring before full micelle
1056 formation[79][80][71][72][81]. In this work, which used the intensity of pyrene fluorescence emission,
1057 two critical concentrations were also detected (Fig S2). The CMC values presented here (Table 4) are
1058 taken from the first break point. The CMC values achieved for F68, P85 and P106 were fairly similar
1059 and did not allow a prioritisation of a specific formulation based on CMC alone. The concentrations of
1060 Pluronic (0.001 to 0.025%) used in the biological assays were based on the CMC values and were
1061 selected on the basis that they would be likely to consist of mainly unimers (0.001-0.025%); a mixture
1062 of unimers and micelles (0.1%) and mostly micelles (0.5%) respectively.

1063

1064 F68 micelles have a relatively small radius of 52.0 Å (Table 7). This attribute will increase stability, half-
1065 life and therefore circulation time of this Pluronic, since small micelles evade detection and
1066 destruction by the reticuloendothelial system. However, this small volume may also correlate to low
1067 drug loading (Table 5; Fig S3). In addition, the fact that pentamidine release from both F68 and P105
1068 micelles is by diffusion would indicate that these Pluronics are unlikely to significantly prolong the
1069 circulation time of pentamidine (Fig S4).

1070

1071 Haemolysis of human red blood cells was not observed in the presence of 0.5%, 0.1%, 0.025%, 0.01%,
1072 and 0.001% P85, P105 or F68, the results being comparable to the negative control (0.05% DMSO).
1073 This suggests that an intravenous formulation containing P85, P105, or F68 would not lead to
1074 haemolysis at the tested concentrations, supporting the safety profile of Pluronic polymers for medical
1075 use[15][82]. In agreement, no differences were reported in the terminal haematological values
1076 (including haemoglobin, packed cell volume, number of erythrocytes, total number of leukocytes) and
1077 blood-chemical values (including urea, total protein, alkaline phosphatase) obtained from rats who
1078 had received once daily intravenous doses of F68 (doses ranging from 10-1000 mg/kg body weight) or
1079 from rats who had been administered physiological saline for one month [83]. No morphological
1080 abnormalities were detected in the rats which received the 0-50 mg/kg daily dose of F68, however,
1081 rats which received the higher doses had detectable alterations i.e. the presence of foam cells in the
1082 lungs (dose was 500-1000 mg/kg) and focal cortical degenerative changes in the kidneys (dose was
1083 100-1000 mg/kg).

1084 Pentamidine caused a concentration-dependent inhibition of insulin secretion from MIN6 β-cells
1085 suggesting that this is one mechanism through which it could induce diabetes[9]. Pentamidine is
1086 known to be an agonist at imidazoline receptors [84], but it is unlikely that this explains its inhibitory
1087 effects on insulin secretion since β-cell imidazoline receptors are coupled to increased insulin
1088 release[85]. However, the imidazoline ligand idazoxan is reported to cause a concentration-
1089 dependent inhibition of β-cell viability[86], similar to the effects observed here with pentamidine, so it
1090 is possible that the reduction in insulin secretion is secondary to pentamidine-mediated activation of
1091 β-cell imidazoline receptors and impairment of cell viability. Pentamidine-induced diabetes is not
1092 thought to be reversible [9], and so testing for a marker of pancreatic off target adverse effects
1093 occurred early in the screening cascade. Importantly, a number of Pluronic formulations (P85, P105)
1094 were shown to increase the peripheral toxicity of pentamidine as measured by decreases in insulin
1095 secretion. In a human tissue cell model (HEK-293), P105 has previously been shown to cause dose

1096 dependent changes in cell viability[16]. However, a lead Pluronic (F68) was identified which
1097 demonstrated equivalent toxicity to unformulated pentamidine, on β-cell viability and insulin
1098 secretion. Supporting this formulation selection our studies also revealed that P85 and P105 at 0.01%
1099 and 0.5% concentrations caused loss of MDCK-MDR monolayer integrity, whereas F68 at
1100 concentrations up to 0.5% had no effect (Fig S7). A correlation between HLB and cytotoxicity has
1101 previously been observed with low cytotoxicity being guaranteed when the HLB of the polymer is ≥10
1102 (Table S1)[28].

1103 Importantly, all formulations tested did not prevent pentamidine killing *Trypanosoma brucei* blood
1104 stream form trypomastigotes. In fact, pure P85 and P105 were highly trypanocidal and F68-
1105 pentamidine formulations had a slight synergistic effect.

1106 *In vitro* BBB studies indicated that there was an efflux process for pentamidine as also demonstrated
1107 in P-gp knockout mice studies [7]. However, we were unable to demonstrate an increase in
1108 pentamidine movement across the barrier in either direction, compared with unformulated
1109 pentamidine in any of our *in vitro* systems.

1110 Further studies utilizing the *in situ* brain perfusion technique confirmed that the Pluronics (P85, P105
1111 or F68) did not increase pentamidine delivery to the brain, including the choroid plexus, after either 10
1112 or 30 minutes exposure. Our studies using *in situ* brain perfusions over 10 minutes in mice have
1113 shown that the P85, P105 and F68 formulations have a tendency to actually prevent uptake of
1114 pentamidine into brain tissue and/or vascular endothelial cells, which constitute an intact BBB. This
1115 may be related to interactions of the Pluronics with influx transporters for pentamidine (e.g. OCT1),
1116 although our *in vitro* BBB studies did not indicate that the pentamidine permeability was affected by
1117 the presence of F68, P85 and P105 (0.01% and 0.1%) in either direction. Importantly, a similar P85
1118 induced reduction in BBB permeability was observed by other workers, [87] who noted a reduction in
1119 the rate of uptake into brain tissue of P85-leptin conjugates during the first 90 minutes after iv
1120 injection compared with native leptin. Despite this initial inhibition of P85-leptin influx, a greater

1121 overall concentration of the conjugate was measured in brain tissue after 4 hours, an observation that
1122 the authors ascribed to improved pharmacokinetic properties. Digoxin delivery to the brain has
1123 previously been determined 1 - 10 hr post-injection in mice and found to be significantly enhanced
1124 when Pluronic 85 is present [88].

1125 Sucrose does not cross phospholipid membranes and was used in the brain perfusion experiments as a
1126 vascular space marker. An increase in [^{14}C(U)]sucrose would indicate that the integrity of the
1127 membrane or the tight junctions between cells had been compromised. Conversely, a decrease would
1128 suggest that the proportionate volume of tissue occupied by blood vessels had been reduced. It is
1129 therefore interesting that F68 has previously been shown to interact with the mechanisms that control
1130 vasoconstriction and vasodilation[89][90] and could lead to the observed reduction in vascular space.

1131

1132 Interestingly, the *in vivo* mouse pharmacokinetic study revealed that the concentrations of
1133 pentamidine in brain parenchyma in this species seem high compared with data from human (using
1134 CSF rather than brain parenchyma) which indicated that less than 1% of the plasma pentamidine
1135 concentration is detected in CSF[91]. Furthermore, assessment of this lead formulation in an *in vivo*
1136 pharmacokinetic study confrmed that F68 did not increase pentamidine delivery to the brain under
1137 the conditions studied. This is not linked to partitioning of pentamidine inside the micelles as this is
1138 low, hence the use of Pluronic micelles to protect this drug after administration and extend its
1139 circulation time is probably limited. Although it may be related to the fact that F68 is hydrophilic and
1140 prefers to remain in the plasma than be distributed to organs [17].

1141

1142 Whilst there are limitations to all assay systems, the package of data generated by the team provided
1143 a compelling and robust data set. The screening cascade has successfully identified Pluronic-
1144 pentamidine formulations that harbour trypanocidal activity and do not increase the safety concerns
1145 centrally or peripherally (over unformulated pentamidine). However, the data suggested that we

1146 would not be able to significantly enhance brain exposure of pentamidine using the Pluronic (F68 , P85
1147 or P105) within a reasonable time frame and existing budget. We therefore drew the study to a close
1148 at milestone 2 (Fig 1). Importantly a significant body of high-quality data has been generated as part
1149 of this project which may be highly relevant to other teams looking to understand block-copolymer
1150 architecture, further develop block-copolymers as nanocarriers, improve BBB penetration of drugs or
1151 to those looking to understand toxicity of pentamidine.
1152

Acknowledgements

This research was funded by a Medical Research Council (MRC) DPFS award (MR/K015451/1) to Dr S.A. Thomas (PI), Dr C.A. Dreiss, Dr C. Lorenz, Professor S. Persaud, Dr M. Christie (all at King's College London), Dr V. Yardley and Professor S. Croft (both at LSHTM). This award was jointly funded by the UK MRC and the UK Department for International Development (DFID) under the MRC/DFID Concordat agreement and is also part of the EDCTP2 programme supported by the European Union. This research was also supported by the MRC (PhD studentship MR/K500811/1) and a multi-user equipment grant from the Wellcome Trust which provided a Perkin-Elmer Tricarb 2900TR liquid scintillation counter (080268). The BBSRC Centre of Integrative Biomedicine provided funding for the haemolysis assay.

We are grateful for the project management support of Dr Gayle Chapman (Biomedical Catalyst Ltd), UK. We would like to acknowledge the support of Dr Surbi Gupta (King's IP & Licensing team) who was involved in the IP assessment of the project.

We would like to acknowledge the support of Drugs for Neglected Diseases initiative (DNDi) a collaborative, patients' needs-driven, non-profit drug research and development organization that is developing new treatments for Neglected Diseases.

We would like to thank Miss Raha Ahmadkhanbeigi (King's College London) for help with the haemolysis assay. We would like to thank Ms Ana-Charlott Berglar (King's College London) for help with acquisition of the preliminary data. We would like to thank ISIS, Rutherford-Appleton Laboratory (Science and Technology Facilities Council, Didcot, Oxford) for the award of neutron beam time on the LOQ instrument to perform the SANS experiments.

1176 **References**

1177 1. Simarro PP, Diarra A, Postigo JAR, Franco JR, Jannin JG. The human african trypanosomiasis control and surveillance programme of the world health
1178 organization 2000-2009: The way forward. PLoS Negl Trop Dis. 2011;5.

1179 2. WHO. No Title. In: http://www.who.int/trypanosomiasis_african/country/en/. 2014.

1180 3. Franco JR, Simarro PP, Diarra A, Jannin JG. Epidemiology of human African trypanosomiasis. Clin Epidemiol. 2014;6: 257–75.
1181 doi:10.2147/CLEP.S39728

1182 4. Sanderson L, Dogruel M, Rodgers J, Bradley B, Thomas SA. The blood-brain barrier significantly limits eflornithine entry into Trypanosoma brucei
1183 brucei infected mouse brain. J Neurochem. 2008;107: 1136–1146.

1184 5. Jeganathan S, Sanderson L, Dogruel M, Rodgers J, Croft S, Thomas SA. The distribution of nifurtimox across the healthy and trypanosome-infected
1185 murine blood-brain and blood-cerebrospinal fluid barriers. J Pharmacol Exp Ther. 2011;336: 506–515.

1186 6. Sanderson L, Khan A, Thomas S. Distribution of suramin, an antitrypanosomal drug, across the blood-brain and blood-cerebrospinal fluid interfaces
1187 in wild-type and P-glycoprotein transporter-deficient mice. Antimicrob Agents Chemother. 2007;51: 3136–3146.

1188 7. Sanderson L, Dogruel M, Rodgers J, Koning HP De, Thomas SA. Pentamidine movement across the murine blood-brain and blood-cerebrospinal fluid
1189 barriers: Effect of trypanosome infection, combination therapy, P-glycoprotein, and multidrug resistance-associated protein. J Pharmacol Exp Ther.
1190 2009;329: 967–971.

1191 8. Doua F, Miezan TW, Singaro JRS, Yapo FB, Baltz T. The efficacy of pentamidine in the treatment of early-late stage Trypanosoma brucei gambiense
1192 trypanosomiasis. Am J Trop Med Hyg. 1996;55: 586–588.

1193 9. Burri C. Chemotherapy against human African trypanosomiasis: is there a road to success? Parasitology. 2010;137: 1987–94.
1194 doi:10.1017/S0031182010001137

1195 10. Batrakova E V, Li S, Li Y, Alakhov VY, Elmquist WF, Kabanov A V. Distribution kinetics of a micelle-forming block copolymer Pluronic P85. J Control
1196 Release. 2004;100: 389–97. doi:10.1016/j.jconrel.2004.09.002

1197 11. Kozlov MY, Melik-Nubarov NS, Batrakova E V., Kabanov A V. Relationship between Pluronic Block Copolymer Structure, Critical Micellization
1198 Concentration and Partitioning Coefficients of Low Molecular Mass Solutes. Macromolecules. American Chemical Society; 2000;33: 3305–3313.
1199 doi:10.1021/ma991634x

1200 12. Cagel M, Tesan FC, Bernabeu E, Salgueiro MJ, Zubillaga MB, Moretton MA, et al. Polymeric mixed micelles as nanomedicines: Achievements and
1201 perspectives. Eur J Pharm Biopharm. 2017;113: 211–228. doi:10.1016/j.ejpb.2016.12.019

1202 13. Oh KT, Bronich TK, Kabanov A V. Micellar formulations for drug delivery based on mixtures of hydrophobic and hydrophilic Pluronic® block
1203 copolymers. J Control Release. 2004;94: 411–422. doi:10.1016/j.jconrel.2003.10.018

1204 14. Chiappetta D.A. and Sosnik A. Poly(ethylene oxide)–poly(propylene oxide) block copolymer micelles as drug delivery agents: Improved
1205 hydrosolubility, stability and bioavailability of drugs. Eur J Pharm Biopharm. 2007;66: 303.

1206 15. Singh-Joy SD, McLain VC. Safety assessment of poloxamers 101, 105, 108, 122, 123, 124, 181, 182, 183, 184, 185, 188, 212, 215, 217, 231, 234, 235,
1207 237, 238, 282, 284, 288, 331, 333, 334, 335, 338, 401, 402, 403, and 407, poloxamer 105 benzoate, and poloxamer 182 dibenzoate as use. Int J
1208 Toxicol. 2008;27 Suppl 2: 93–128. doi:10.1080/10915810802244595

1209 16. Fang X, Chen, Sha X, Zhang, Zhong, Fan, et al. Pluronic mixed micelles overcoming methotrexate multidrug resistance: in vitro and in vivo evaluation.
1210 Int J Nanomedicine. 2013; 1463. doi:10.2147/IJN.S42368

1211 17. Alakhov VY, Kabanov A V. Block copolymeric biotransport carriers as versatile vehicles for drug delivery. Expert Opin Investig Drugs. 1998;7: 1453–
1212 1473. doi:10.1517/13543784.7.9.1453

1213 18. Shaik N, Pan G, Elmquist WF. Interactions of pluronic block copolymers on P-gp efflux activity: Experience with HIV-1 protease inhibitors. J Pharm Sci.
1214 2008;97: 5421–5433. doi:10.1002/jps.21372

1215 19. Batrakova E V., Han H-Y, Alakhov VY, Miller DW, Kabanov A V. Effects of Pluronic Block Copolymers on Drug Absorption in Caco-2 Cell Monolayers.
1216 Pharm Res. Kluwer Academic Publishers-Plenum Publishers; 1998;15: 850–855. doi:10.1023/A:1011964213024

1217 20. Batrakova E, Lee S, Li S, Venne A, Alakhov V, Kabanov A. Fundamental Relationships Between the Composition of Pluronic Block Copolymers and
1218 Their Hypersensitization Effect in MDR Cancer Cells. Pharm Res. 1999;16: 1373–1379. doi:10.1023/A:1018942823676

1219 21. Shaik N, Giri N, Elmquist WF. Investigation of the micellar effect of pluronic P85 on P-glycoprotein inhibition: cell accumulation and equilibrium
1220 dialysis studies. J Pharm Sci. 2009;98: 4170–90. doi:10.1002/jps.21723

1221 22. Miller DW, Batrakova E V., Kabanov A V. Inhibition of Multidrug Resistance-Associated Protein (MRP) Functional Activity with Pluronic Block
1222 Copolymers. Pharm Res. Kluwer Academic Publishers-Plenum Publishers; 1999;16: 396–401. doi:10.1023/A:1018873702411

1223 23. Rapoport N, Marin AP, Timoshin AA. Effect of a Polymeric Surfactant on Electron Transport in HL-60 Cells. Arch Biochem Biophys. 2000;384: 100–
1224 108. doi:10.1006/abbi.2000.2104

1225 24. Batrakova E V. Optimal Structure Requirements for Pluronic Block Copolymers in Modifying P-glycoprotein Drug Efflux Transporter Activity in Bovine
1226 Brain Microvessel Endothelial Cells. J Pharmacol Exp Ther. 2003;304: 845–854. doi:10.1124/jpet.102.043307

1227 25. Wang Y, Hao J, Li Y, Zhang Z, Sha X, Han L, et al. Poly(caprolactone)-modified Pluronic P105 micelles for reversal of paclitaxcel-resistance in SKOV-3
1228 tumors. Biomaterials. 2012;33: 4741–51. doi:10.1016/j.biomaterials.2012.03.013

1229 26. Venne A, Li S, Mandeville R, Kabanov A, Alakhov V. Hypersensitizing effect of pluronic L61 on cytotoxic activity, transport, and subcellular
1230 distribution of doxorubicin in multiple drug- resistant cells. Cancer Res. 1996;56: 3626–3629.

1231 27. Huang J, Si L, Jiang L, Fan Z, Qiu J, Li G. Effect of pluronic F68 block copolymer on P-glycoprotein transport and CYP3A4 metabolism. Int J Pharm.
1232 2008;356: 351–3. doi:10.1016/j.ijpharm.2007.12.028

1233 28. Budkina OA, Demina T V., Dorodnykh TY, Melik-Nubarov NS, Grozdova ID. Cytotoxicity of nonionic amphiphilic copolymers. Polym Sci Ser A. 2012;54:
1234 707–717. doi:10.1134/S0965545X12080020

1235 29. Valle JW, Armstrong A, Newman C, Alakhov V, Pietrzynski G, Brewer J, et al. A phase 2 study of SP1049C, doxorubicin in P-glycoprotein-targeting
1236 pluronics, in patients with advanced adenocarcinoma of the esophagus and gastroesophageal junction. Invest New Drugs. 2011;29: 1029–1037.

1237 30. Alakhova DY, Zhao Y, Li S, Kabanov A V. Effect of Doxorubicin/Pluronic SP1049C on Tumorigenicity, Aggressiveness, DNA Methylation and Stem Cell
1238 Markers in Murine Leukemia. PLoS One. 2013;8. doi:10.1371/journal.pone.0072238

1239 31. Mendonça DVC, Lage LMR, Lage DP, Chávez-Fumagalli MA, Ludolf F, Roatt BM, et al. Poloxamer 407 (Pluronic® F127)-based polymeric micelles for
1240 amphotericin B: In vitro biological activity, toxicity and in vivo therapeutic efficacy against murine tegumentary leishmaniasis. Exp Parasitol.
1241 2016;169: 34–42. doi:10.1016/j.exppara.2016.07.005

1242 32. Alakhova DY, Kabanov A V. Pluronics and MDR reversal: an update. Mol Pharm. 2014;11: 2566–78. doi:10.1021/mp500298q

1243 33. Zhang K, Khan A. Phase Behavior of Poly(ethylene oxide)-Poly(propylene oxide)-Poly(ethylene oxide) Triblock Copolymers in Water. Macromolecules.
1244 1995;28: 3807–3812. doi:10.1021/ma00115a009

1245 34. World Health Organization. Stability testing of active pharmaceutical ingredients and finished pharmaceutical products. WHO Tech Rep Ser.
1246 2009;953: 87–130. Available: http://www.ich.org/fileadmin/Public_Web_Site/ICH_Products/Guidelines/Quality/Q1F/Stability_Guideline_WHO.pdf

1247 35. Fu Y, Kao WJ. Drug release kinetics and transport mechanisms of non-degradable and degradable polymeric delivery systems. Expert Opin Drug
1248 Deliv. 2010;7: 429–444. doi:10.1517/17425241003602259

1249 36. Gaitano GG, Brown W, Tardajos G. Inclusion Complexes between Cyclodextrins and Triblock Copolymers in Aqueous Solution: A Dynamic and Static
1250 Light-Scattering Study. J Phys Chem B. 1997;101: 710–719. doi:10.1021/jp961996w

1251 37. Chiappetta DA, Sosnik A. Poly(ethylene oxide)–poly(propylene oxide) block copolymer micelles as drug delivery agents: Improved hydrosolubility,

1252 stability and bioavailability of drugs. Eur J Pharm Biopharm. 2007;66: 303–317. doi:10.1016/j.ejpb.2007.03.022

1253 38. Heenan, R K; King, S.M., Osborn, R., Stanley HB. COLETTE Users Guide, Rutherford Appleton Laboratory Report. Rutherford Applet Lab Rep. 1989;
1254 89–128.

1255 39. King, S.M., Heenan RK. Using COLETTE. Rutherford Applet Lab Rep. 1995;95.

1256 40. SasView [Internet]. [cited 23 Nov 2014]. Available: http://www.sasview.org/

1257 41. Warren PB. Dissipative particle dynamics. Curr Opin Colloid Interface Sci. 1998;3: 620–624. doi:10.1016/S1359-0294(98)80089-7

1258 42. Chen S, Guo C, Hu G-H, Liu H-Z, Liang X-F, Wang J, et al. Dissipative particle dynamics simulation of gold nanoparticles stabilization by PEO–PPO–PEO
1259 block copolymer micelles. Colloid Polym Sci. 2007;285: 1543–1552. doi:10.1007/s00396-007-1721-x

1260 43. Neun BW, Dobrovolskaia MA. Method for analysis of nanoparticle hemolytic properties in vitro. Methods Mol Biol. 2011;697: 215–24.
1261 doi:10.1007/978-1-60327-198-1_23

1262 44. Persaud SJ, Roderigo-Milne HM, Squires PE, Sugden D, Wheeler-Jones CPD, Marsh PJ, et al. A key role for beta-cell cytosolic phospholipase A(2) in
1263 the maintenance of insulin stores but not in the initiation of insulin secretion. Diabetes. 2002;51: 98–104. Available:
1264 http://www.ncbi.nlm.nih.gov/pubmed/11756328

1265 45. Jones PM, Salmon DM, Howell SL. Protein phosphorylation in electrically permeabilized islets of Langerhans. Effects of Ca2+, cyclic AMP, a phorbol
1266 ester and noradrenaline. Biochem J. 1988;254: 397–403. Available: http://www.ncbi.nlm.nih.gov/pubmed/2845950

1267 46. Persaud, S.J., Al-Majed, H., Raman, A. JPM. Gymnema sylvestre stimulates insulin release in vitro by increased membrane permeability. J Endocrinol.
1268 1999;163: 207–212. doi:10.1677/joe.0.1630207

1269 47. Thomas née Williams SA, Segal MB. Identification of a saturable uptake system for deoxyribonucleosides at the blood-brain and blood-cerebrospinal
1270 fluid barriers. Brain Res. 1996;741: 230–239. doi:10.1016/S0006-8993(96)00930-4

1271 48. Williams SA, Abbruscato TJ, Hruby VJ, Davis TP. Passage of a delta-opioid receptor selective enkephalin, [D-penicillamine2,5] enkephalin, across the
1272 blood-brain and the blood-cerebrospinal fluid barriers. J Neurochem. 1996;66: 1289–99. Available: http://www.ncbi.nlm.nih.gov/pubmed/8769896

1273 49. Sanderson L, Khan A, Thomas S. Distribution of suramin, an antitrypanosomal drug, across the blood-brain and blood-cerebrospinal fluid interfaces
1274 in wild-type and P-glycoprotein transporter-deficient mice. Antimicrob Agents Chemother. 2007;51: 3136–3146.

1275 50. Thomas née Williams SA, Segal MB. Identification of a saturable uptake system for deoxyribonucleosides at the blood-brain and blood-cerebrospinal

1276 fluid barriers. Brain Res. 1996;741: 230–239. doi:10.1016/S0006-8993(96)00930-4

1277 51. Triguero D, Buciak J, Pardridge WM. Capillary depletion method for quantification of blood-brain barrier transport of circulating peptides and plasma
1278 proteins. J Neurochem. 1990;54: 1882–8.

1279 52. Räz B, Iten M, Grether-Bühler Y, Kaminsky R, Brun R. The Alamar Blue assay to determine drug sensitivity of African trypanosomes (T.b. rhodesiense
1280 and T.b. gambiense) in vitro. Acta Trop. 1997;68: 139–47. Available: http://www.ncbi.nlm.nih.gov/pubmed/9386789

1281 53. Miézan TW, Bronner U, Doua F, Cattand P, Rombo L. Long-term exposure of Trypanosoma brucei gambiense to pentamidine in vitro. Trans R Soc
1282 Trop Med Hyg. 88: 332–3. Available: http://www.ncbi.nlm.nih.gov/pubmed/7974681

1283 54. Wood DH, Hall JE, Rose BG, Tidwell RR. 1,5-Bis(4-amidinophenoxy)pentane (pentamidine) is a potent inhibitor of []idazoxan binding to imidazoline I2
1284 binding sites. Eur J Pharmacol. 1998;353: 97–103. doi:10.1016/S0014-2999(98)00386-0

1285 55. De Boer T, Nalos L, Stary A, Kok B, Houtman M, Antoons G, et al. The anti-protozoal drug pentamidine blocks KIR2.x-mediated inward rectifier
1286 current by entering the cytoplasmic pore region of the channel. Br J Pharmacol. 2010;159: 1532–1541. doi:10.1111/j.1476-5381.2010.00658.x

1287 56. Nalos L, de Boer TP, Houtman MJC, Rook MB, Vos MA, van der Heyden MAG. Inhibition of lysosomal degradation rescues pentamidine-mediated
1288 decreases of K(IR)2.1 ion channel expression but not that of K(v)11.1. Eur J Pharmacol. 2011;652: 96–103. doi:10.1016/j.ejphar.2010.10.093

1289 57. Williams K, Dattilo M, Sabado TN, Kashiwagi K, Igarashi K. Pharmacology of delta2 glutamate receptors: effects of pentamidine and protons. J
1290 Pharmacol Exp Ther. 2003;305: 740–8. doi:10.1124/jpet.102.045799

1291 58. Cox D, Motoyama Y, Seki J, Aoki T, Dohi M YK. Pentamidine: a non-peptide GPIIb/IIIa antagonist--in vitro studies on platelets from humans and other
1292 species. Thromb Haemost. 1992;68: 731–736.

1293 59. Reynolds IJ, Aizenman E. Pentamidine is an N-methyl-D-aspartate receptor antagonist and is neuroprotective in vitro. J Neurosci. 1992;12: 970–5.
1294 Available: http://www.ncbi.nlm.nih.gov/pubmed/1532027

1295 60. Pathak MK, Dhawan D, Lindner DJ, Borden EC, Farver C, Yi T. Pentamidine is an inhibitor of PRL phosphatases with anticancer activity. Mol Cancer
1296 Ther. 2002;1: 1255–64. Available: http://www.ncbi.nlm.nih.gov/pubmed/12516958

1297 61. Kitamura Y, Arima T, Imaizumi R, Sato T, Nomura Y. Inhibition of constitutive nitric oxide synthase in the brain by pentamidine, a calmodulin
1298 antagonist. Eur J Pharmacol. 1995;289: 299–304. Available: http://www.ncbi.nlm.nih.gov/pubmed/7542607

1299 62. Chen X, Qiu L, Li M, D??rrnagel S, Orser BA, Xiong ZG, et al. Diarylamidines: High potency inhibitors of acid-sensing ion channels.
1300 Neuropharmacology. 2010;58: 1045–1053. doi:10.1016/j.neuropharm.2010.01.011

1301 63. Perilo CS, Pereira MT, Santoro MM, Nagem RAP. Structural binding evidence of the trypanocidal drugs berenil and pentacarinate active principles to
1302 a serine protease model. Int J Biol Macromol. 2010;46: 502–11. doi:10.1016/j.ijbiomac.2010.03.006

1303 64. Cimecioglu AL, Weiss RA. Aromatic Polyamides of 3,8-Diamino-6-phenylphenanthridine and Their Molecular Complexes with Sulfonated Polystyrene
1304 Ionomers. Macromolecules. 1995;28: 6343–6346. doi:10.1021/ma00122a047

1305 65. Mortensen K, Brown W. Poly(ethylene oxide)-poly(propylene oxide)-poly(ethylene oxide) triblock copolymers in aqueous solution. The influence of
1306 relative block size. Macromolecules. 1993;26: 4128–4135. doi:10.1021/ma00068a010

1307 66. Hammouda B. SANS from Pluronic P85 in d-water. Eur Polym J. 2010;46: 2275–2281. doi:10.1016/j.eurpolymj.2010.10.012

1308 67. Valero M, Castiglione F, Mele A, da Silva MA, Grillo I, González-Gaitano G, et al. Competitive and Synergistic Interactions between Polymer Micelles,
1309 Drugs, and Cyclodextrins: The Importance of Drug Solubilization Locus. Langmuir. 2016;32: 13174–13186. doi:10.1021/acs.langmuir.6b03367

1310 68. Puig-Rigall J, Obregon-Gomez I, Monreal-Pérez P, Radulescu A, Blanco-Prieto MJ, Dreiss CA, et al. Phase behaviour, micellar structure and linear
1311 rheology of tetrablock copolymer Tetronic 908. J Colloid Interface Sci. 2018;524: 42–51. doi:10.1016/j.jcis.2018.03.096

1312 69. Wanka G, Hoffmann H, Ulbricht W. Phase Diagrams and Aggregation Behavior of Poly(oxyethylene)-Poly(oxypropylene)-Poly(oxyethylene) Triblock
1313 Copolymers in Aqueous Solutions. Macromolecules. 1994;27: 4145–4159. doi:10.1021/ma00093a016

1314 70. Alexandridis P, Alan Hatton T. Poly(ethylene oxide)�poly(propylene oxide)�poly(ethylene oxide) block copolymer surfactants in aqueous solutions
1315 and at interfaces: thermodynamics, structure, dynamics, and modeling. Colloids Surfaces A Physicochem Eng Asp. 1995;96: 1–46. doi:10.1016/0927-
1316 7757(94)03028-X

1317 71. Alexandridis P, Holzwarth JF, Hatton TA. Micellization of Poly(ethylene oxide)-Poly(propylene oxide)-Poly(ethylene oxide) Triblock Copolymers in
1318 Aqueous Solutions: Thermodynamics of Copolymer Association. Macromolecules. 1994;27: 2414–2425. doi:10.1021/ma00087a009

1319 72. Alexandridis P, Athanassiou V, Fukuda S, Hatton TA. Surface Activity of Poly(ethylene oxide)-block-Poly(propylene oxide)-block-Poly(ethylene oxide)
1320 Copolymers. Langmuir. 1994;10: 2604–2612. doi:10.1021/la00020a019

1321 73. Lopes JR, Loh W. Investigation of Self-Assembly and Micelle Polarity for a Wide Range of Ethylene Oxide−Propylene Oxide−Ethylene Oxide Block
1322 Copolymers in Water. Langmuir. 1998;14: 750–756. doi:10.1021/la9709655

1323 74. Booth C, Attwood D. Effects of block architecture and composition on the association properties of poly(oxyalkylene) copolymers in aqueous
1324 solution. Macromol Rapid Commun. 2000;21: 501–527. doi:10.1002/1521-3927(20000601)21:9<501::AID-MARC501>3.0.CO;2-R

1325 75. Pepić I, Lovrić J, Hafner A, Filipović-Grčić J. Powder form and stability of Pluronic mixed micelle dispersions for drug delivery applications. Drug Dev

1326 Ind Pharm. 2014;40: 944–951. doi:10.3109/03639045.2013.791831

1327 76. Wanka G, Hoffmann H, Ulbricht W. The aggregation behavior of poly-(oxyethylene)-poly-(oxypropylene)-poly-(oxyethylene)-block-copolymers in
1328 aqueous solution. Colloid Polym Sci. 1990;268: 101–117. doi:10.1007/BF01513189

1329 77. Kositza MJ, Bohne C, Alexandridis P, Hatton TA, Holzwarth JF. Micellization Dynamics and Impurity Solubilization of the Block-Copolymer L64 in an
1330 Aqueous Solution. Langmuir. 1999;15: 322–325. doi:10.1021/la9812368

1331 78. Loh W. Block and Copolymer Micelles. In: Somasundaram, P., Dekker M, editor. Encyclopedia of Surface and Colloid Science. 2006. pp. 1014–1025.

1332 79. Prasad KN, Luong TT, FlorenceJoelle Paris AT, Vaution C, Seiller M, Puisieux F. Surface activity and association of ABA polyoxyethylene—
1333 polyoxypropylene block copolymers in aqueous solution. J Colloid Interface Sci. 1979;69: 225–232. doi:10.1016/0021-9797(79)90151-6

1334 80. Sahoo L, Sarangi J, Misra PK. Organization of Amphiphiles, Part 1: Evidence in Favor of Pre-micellar Aggregates through Fluorescence Spectroscopy.
1335 Bull Chem Soc Jpn. 2002;75: 859–865. doi:10.1246/bcsj.75.859

1336 81. Kabanov A V., Nazarova IR, Astafieva I V., Batrakova E V., Alakhov VY, Yaroslavov AA, et al. Micelle Formation and Solubilization of Fluorescent
1337 Probes in Poly(oxyethylene-b-oxypropylene-b-oxyethylene) Solutions. Macromolecules. American Chemical Society; 1995;28: 2303–2314.
1338 doi:10.1021/ma00111a026

1339 82. Lowe KC, Furmidge BA, Thomas S. Haemolytic Properties of Pluronic Surfactants and Effects of Purification. Artif Cells, Blood Substitutes, Biotechnol.
1340 1995;23: 135–139. doi:10.3109/10731199509117673

1341 83. Magnusson G, Olsson T, Nyberg JA. Toxicity of Pluronic F-68. Toxicol Lett. 1986;30: 203–7. Available: http://www.ncbi.nlm.nih.gov/pubmed/3705104

1342 84. Morgan N, Chan S. Imidazoline Binding Sites in the Endocrine Pancreas: Can They Fulfil Their Potential as Targets for the Development of New Insulin
1343 Secretagogues? Curr Pharm Des. 2001;7: 1413–1431. doi:10.2174/1381612013397366

1344 85. Morgan NG. Imidazoline receptors: new targets for antihyperglycaemic drugs. Expert Opin Investig Drugs. 1999;8: 575–84.
1345 doi:10.1517/13543784.8.5.575

1346 86. Gao H, Mourtada M, Morgan NG. Effects of the imidazoline binding site ligands, idazoxan and efaroxan, on the viability of insulin-secreting BRIN-
1347 BD11 cells. JOP. 2003;4: 117–24. Available: http://www.ncbi.nlm.nih.gov/pubmed/12743417

1348 87. Yi X, Yuan D, Farr SA, Banks WA, Poon C-D, Kabanov A V. Pluronic modified leptin with increased systemic circulation, brain uptake and efficacy for
1349 treatment of obesity. J Control Release. 2014;191: 34–46. doi:10.1016/j.jconrel.2014.05.044

1350 88. Batrakova E V, Miller DW, Li S, Alakhov VY, Kabanov A V, Elmquist WF. Pluronic P85 enhances the delivery of digoxin to the brain: in vitro and in vivo
1351 studies. J Pharmacol Exp Ther. 2001;296: 551–7. Available: http://www.ncbi.nlm.nih.gov/pubmed/11160643

1352 89. Saeed M, Hartmann A, Bing RJ. Inhibition of vasoactive agents by perfluorochemical emulsion. Life Sci. 1987;40: 1971–9. Available:
1353 http://www.ncbi.nlm.nih.gov/pubmed/2437426

1354 90. Watanabe M, Okada T. Lysophosphatidylcholine-induced myocardial damage is inhibited by pretreatment with poloxamer 188 in isolated rat heart.
1355 Mol Cell Biochem. 2003;248: 209–15. Available: http://www.ncbi.nlm.nih.gov/pubmed/12870676

1356 91. Bronner U, Doua F, Ericsson Ö, Gustafsson LL, Miézan T, Rais M, et al. Pentamidine concentrations in plasma, whole blood and cerebrospinal fluid
1357 during treatment of Trypanosoma gambiense infection in Côte d'Ivoire. Trans R Soc Trop Med Hyg. 1991;85: 608–611. doi:10.1016/0035-
1358 9203(91)90364-5

1359

1360

1361 **Supporting information captions**

1362 **Fig S1. Pentamidine is returned to the blood from the capillary endothelial cell by P-gp and MRP. Pluronic® P85 inhibits-mediated efflux (e.g. P-gp and**
1363 **MRP transport) by two mechanisms; the first through membrane fluidisation and the second through transient ATP depletion**. These effects are believed
1364 to be mediated by unimers (single polymer chains) [21][19]. Inhibition of efflux should facilitate the accumulation of pentamidine in the human cerebral
1365 capillary endothelium and the murine choroid plexus epithelium, leading to higher concentrations of pentamidine.

1366 **Fig S2. Pyrene fluorescence intensity dependence on pluronic concentration for F68, P85 and P105**. The CMC was determined using 18 different
1367 concentrations (range 0.0001 to 1 w/v%) of pure P85, P105 and F68. The value at each concentration is the mean of two samples, each prepared from a
1368 separate preparation of the stock solution. As expected the curves show two inflection points. The first was taken as the CMC.

1369

1370 **Fig S3. Typical partition data for PTI fluorescence as a function of F68 and P105 concentration.**

1371

1372 **Fig S4. Drug release from dialysis cells measured over time. The experiments were conducted in water at 37°C for concentrations as close as possible to**
1373 ***in vitro* conditions, within experimental limitations, namely, 1% w/v of Pluronics and 10mM PTI**. No significant differences between the Pluronics were
1374 observed and drug release is diffusion controlled (Fickian diffusion) under the experimental conditions. Pluronics micelles are not a barrier to drug release.

1375

1376 **Fig S5: SANS Pluronic data at 37°C.** A) P85 5% B) F68 5% C) P85 5% / PTI 1 % D) F68 5% / PTI 1 % E) P85 5% / PTI 3 % F) F68 5% / PTI 3 %.

1377

1378 **Fig S6. The average number of Pluronic molecules found in a micelle (N_{agg}) and the number of micelles in our system (after they have**
1379 **equilibrated) (N_{mic}) as a function of the concentration of the F68 Pluronic in a system that contains F68 and 0.01 w/v% of L61 Pluronic**. In
1380 the both plots, the black curve represents the results when considering both the L61 and F68 polymers in the mixture, and the blue dashed
1381 curve represents the data from the pure F68 simulated systems. In the top curve, the red curve represents the number of F68 in a micelle
1382 which contains both F68 and L61, and the green curve represents the number of L61 in a micelle. The results show that as we increase the
1383 concentration of F68, and therefore make the system more and more like the pure F68 system, the number of polymer molecules in a micelle and the
1384 number of micelles converge to that observed in the pure F68 system, as expected. Interestingly, it seems that from our simulations that L61 causes the
1385 aggregation of F68 to become slightly enhanced as the number of F68 in the average micelle is always larger than that found in the pure F68 micelles, which
1386 naturally results in their being fewer micelles.

1387 **Fig S7. Apical to basolateral permeability of [^{14}C]sucrose in the presence of P85, P105, and F68 concentrations measured over 60 minutes**. Significant
1388 differences compared to control (no pluronic) was observed in the presence of P85 and P105 (***$p<0.001$, **$p<0.01$). All data are expressed as mean ±
1389 S.E.M, n= 3 wells. Data were analysed using one-way ANOVA with SigmaPlot 13.0.

1390

1391 **Fig S8. Effects of exposure of MIN6 β-cells to 0 (control), 1 or 100 μM pentamidine for 3 and 24 hours. Trypan blue uptake.** Blue staining demonstrates

1392 cells of compromised viability, highlighting the toxicity of 100 μM pentamidine to these cells after 3 hours exposure.

1393

1394 **Fig S9. Effects of exposure of MIN6 β-cells to 0, 1, 10 or 100 μM pentamidine and 0, 0.01, 0.025, 0.1 or 0.5% w/v% F68 for 24 hours**. Trypan blue uptake.

1395 Blue staining demonstrates cells of compromised viability, highlighting the toxicity of 100 μM pentamidine and 0.5% F68 to these cells.

1396

1397 **Table S1. Single point CNS screening of pentamidine at a concentration of 1.0E^{-5} M (PE study no. 13-9625).** Values are expressed as the percent inhibition

1398 of specific binding and represent the average of replicate tubes. Bolder values represent inhibition of 50% or greater.

1399 **Table S2. Inhibition of hKir2.1 potassium channel activity with pentamidine isethionate.**

1400 **Evaluated by the QPatch HT an automatic parallel patch clamp system.** The duration of exposure to each test concentration was 3 minutes.

1401

1402 **Table S3. A visual evaluation of the phase separation of Pluronics dispersions in pure water. Transparent is fully transparent. Opaque**

1403 **completely blocks light.** Slight indicates for slightly translucent (faintly white tint in the solution), and medium indicates obvious translucence.

1404 **Table S4. A visual evaluation of the phase separation of pluronics dispersions in saline. Transparent is fully transparent**. Opaque completely blocks light.

1405 Slight indicates for slightly translucent (faintly white tint in the solution), and medium indicates obvious translucence

1406 **Table S5. The effect of P85, F68 and P105 on the apparent permeability of pentamidine isethionate across MDR1-MDCK cell monolayers in the**
1407 **basolateral to apical direction.** The apical to basolateral movement of pentamidine isethionate was below the limits of detection. The percentage
1408 recovery of pentamidine isethionate is also shown. Lucifer yellow permeation was below 0.5 x 10^{-6} cm/s in all experiments confirming the integrity of the
1409 monolayer. Transcellular marker (propranolol) and Pgp and BCRP substrate (prazosin) apparent permeability values are also shown.

1410 **Table S6. The effect of Pluronic P85 on the accumulation of [^{3}H(G)]pentamidine (15.7 nM) into brain tissues after 10 minutes of *in situ* perfusion.** All
1411 values have been corrected for vascular space by subtraction of the R_{TISSUE}% for [^{14}C(U)]sucrose from the R_{TISSUE}% for [^{3}H(G)]pentamidine. All values mean ±
1412 SEM.

1413 **Table S7. The effect of Pluronic P105 on the accumulation of [^{3}H(G)]pentamidine (15.7 nM) into brain parenchyma after 10 minutes of *in situ***
1414 **perfusion.** All values have been corrected for vascular space by subtraction of the R_{TISSUE}% for [^{14}C(U)] sucrose from the R_{TISSUE}% for [^{3}H(G)]pentamidine.

1415 **Table S8. Accumulation of ^{3}H-pentamidine (15.7 nM) after 10 minutes perfusion with or without pluronic F68 (not corrected for vascular space; Control A**
1416 **and 0.01% and 0.1% F68 experiments were carried out using MP Biomedicals dextran.** Control B and 0.5% F68 experiments were carried out
1417 using VWR dextran).

1418 **Table S9. Accumulation of [^{14}C]sucrose after 10 minutes perfusion with or without Pluronic F68; Control A and 0.01% and 0.1% F68 experiments were**
1419 **carried out using MP Biomedicals dextran.** Control B and 0.5% F68 experiments were carried out using VWR dextran).

1420 **Table S10A. Accumulation of [^{3}H]pentamidine after 30 minutes perfusion with or without pluronic F68**. (Not corrected for vascular space).

1421 **Table S10B. Accumulation of [^{14}C]sucrose (B) after 30 minutes perfusion with or without pluronic F68.** (Not corrected for vascular space).

1422

START

Perkin-Elmer CNS neurological profiling screen

Chantest ion channel screen

For ~ 30 Formulations

SAR feedback loop

In silico
Critical Micellar Concentration (CMC)
Hydration stability
Encapsulation efficiency

Additional Formulation Studies
- SANS; Aggregate structure
- SANS/NMR/Fluo; Aggregation number
- NMR: drug/polymer interaction
- *In* silico: Aggregate structure, aggregation number, drug/polymer interaction, polymer/P-gp interaction

Physical Properties in vitro
Critical Micellar Concentration (CMC)
Formulation Stability (37°)
Drug Release studies (dialysis)
Drug Partitioning (Fluorescence)

BBB penetration
Human BBB EC uptake *in vitro*
Mouse choroid plexus delivery *in vivo*

Peripheral Toxicity in vitro
- Haemolysis assay
- Beta cell viability & Insulin secretion
- 72h exposure *cf* pentamidine alone

Trypanocidal Activity in vitro
Trypanosomal killing
72h exposure *cf* pentamidine alone

Milestone 1 (at 12 months): Select at least 5-6 formulations for further characterisation

Human EC toxicity (MTT) *in vitro*

Formulation viscosity/stability

Mouse neuronal toxicity *in vitro*

Mouse Irwin screen *in vivo*

Brain penetration in vivo (mouse; i.v.)
Plasma & terminal brain samples
Pentamidine brain:plasma ratio

CSF penetration in vivo (mouse; i.v.)
- Plasma & microdialysis samples
- Pentamidine CSF:plasma ratio

All shaded boxes=CROs/Outsourced experiments

Multiple dose studies in vivo (mouse; i.v.)
Plasma & terminal brain samples
Steady state pentamidine brain:plasma ratio

Milestone 2 (24 months): Select 1-2 formulations for efficacy and toxicity studies *in vivo*

Efficacy against Stage 1 HAT (mouse; i.v.)
- 1 month model
- Bioanalysis; terminal brain & plasma samples

Efficacy against Stage 2 HAT (mouse; i.v.)
3 month model (in vivo imaging)
Bioanalysis; terminal brain & plasma samples

Peripheral Toxicity in vivo (mouse; i.v.)
Glucose tolerance , insulin secretion
Pancreas/brain histopathology

Milestone 3 (30 months): Identify 1 formulation that is effective against stage 2 HAT

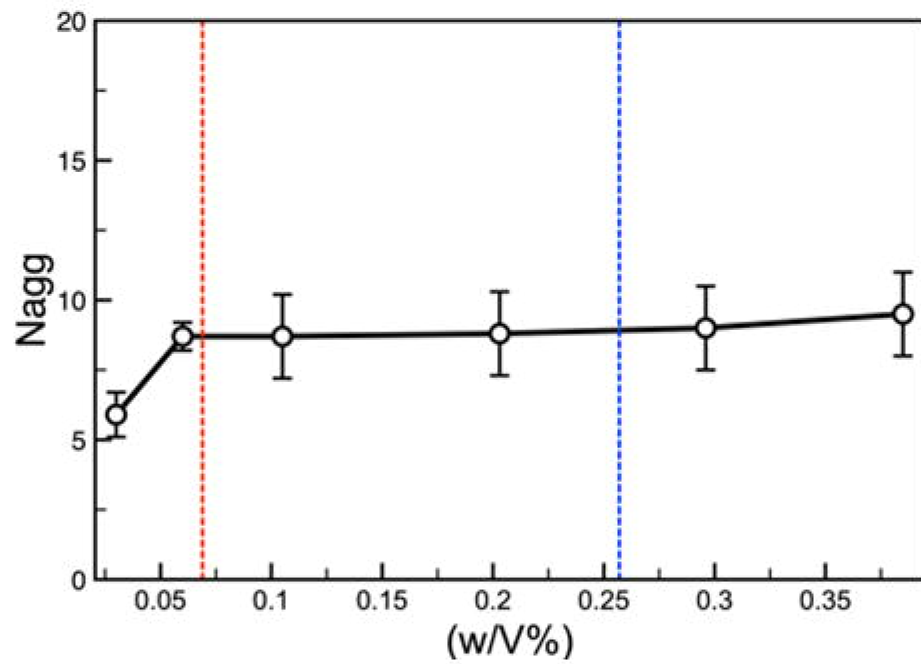
Nagg
(w/V%)

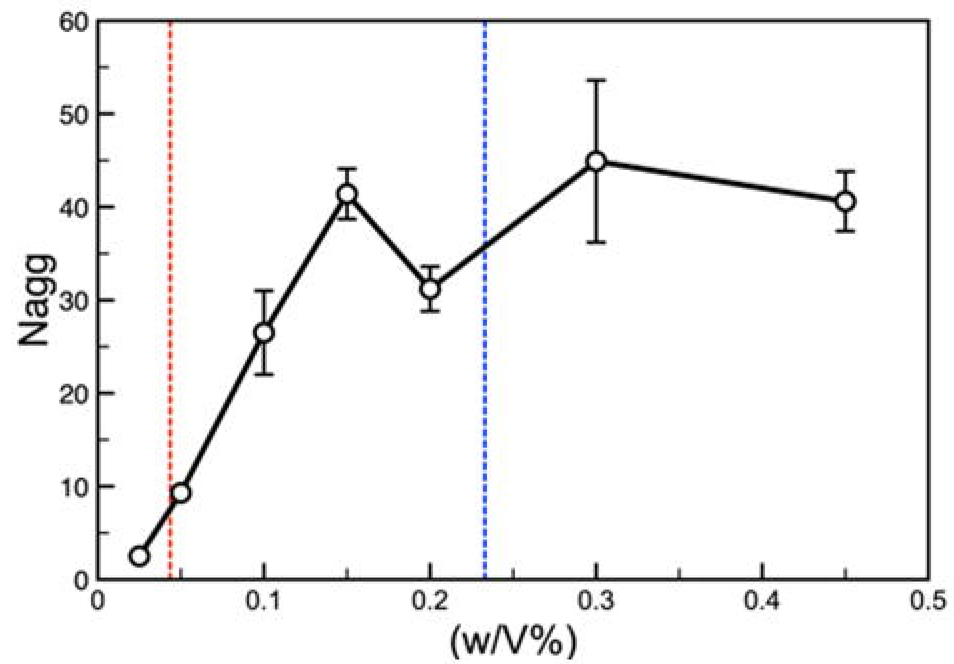
Nagg
(w/V%)

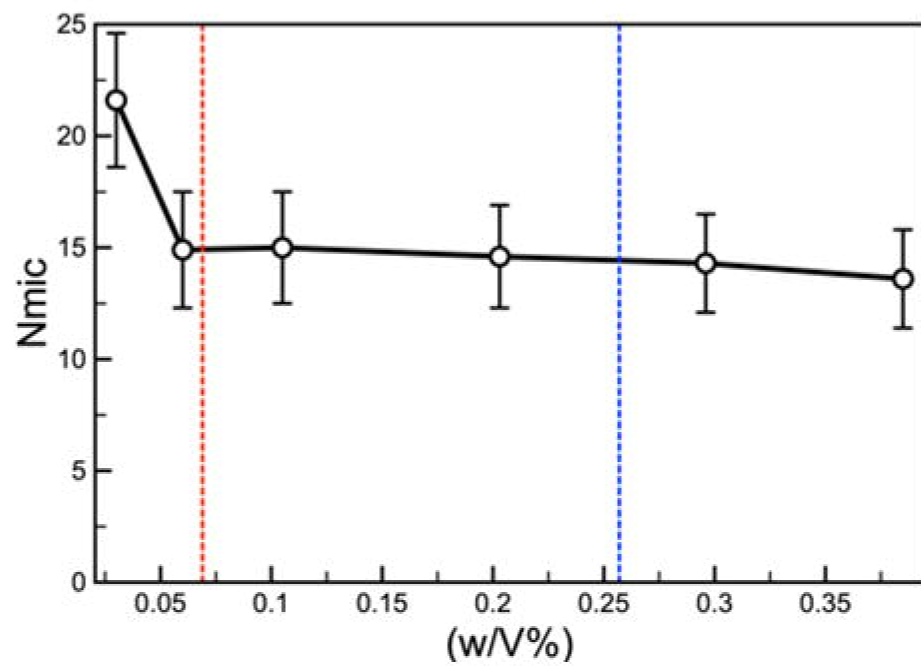
Nmic
(w/V%)

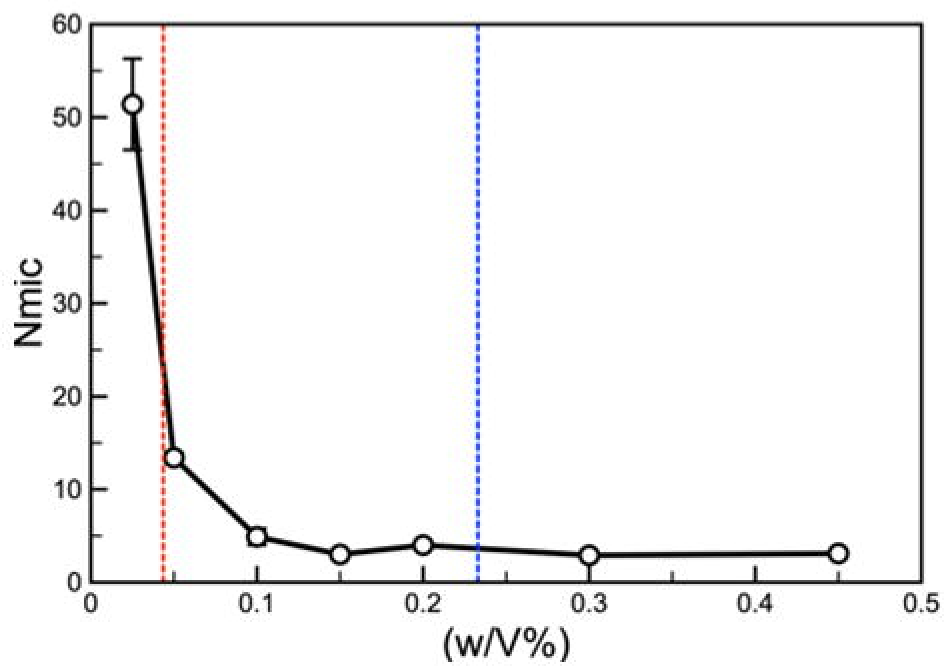
Nmic
(w/V%)

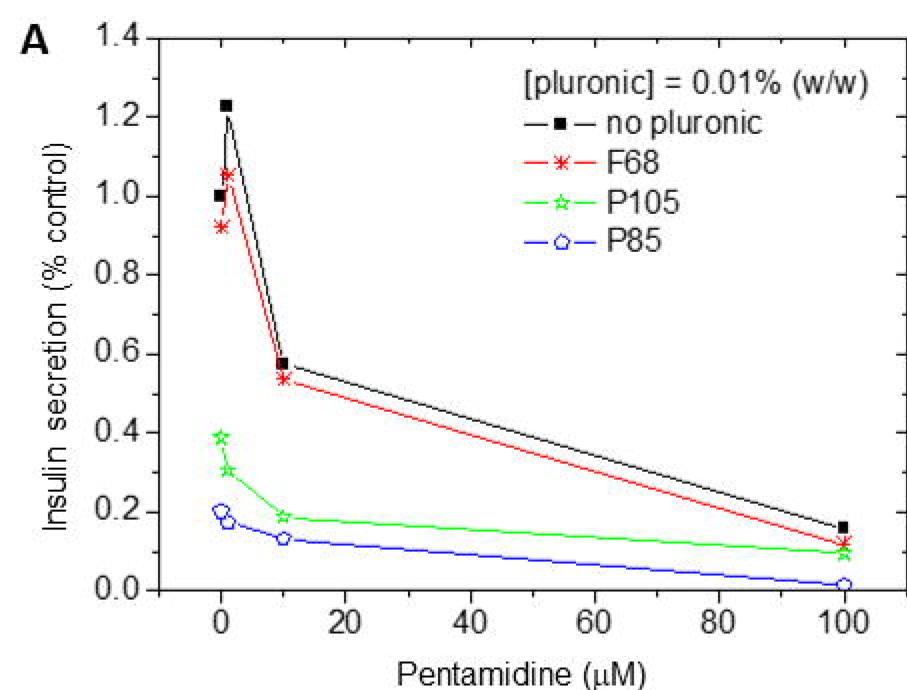
A
[pluronic] = 0.01% (w/w)
no pluronic
F68
P105
P85
Insulin secretion (% control)
Pentamidine (μM)

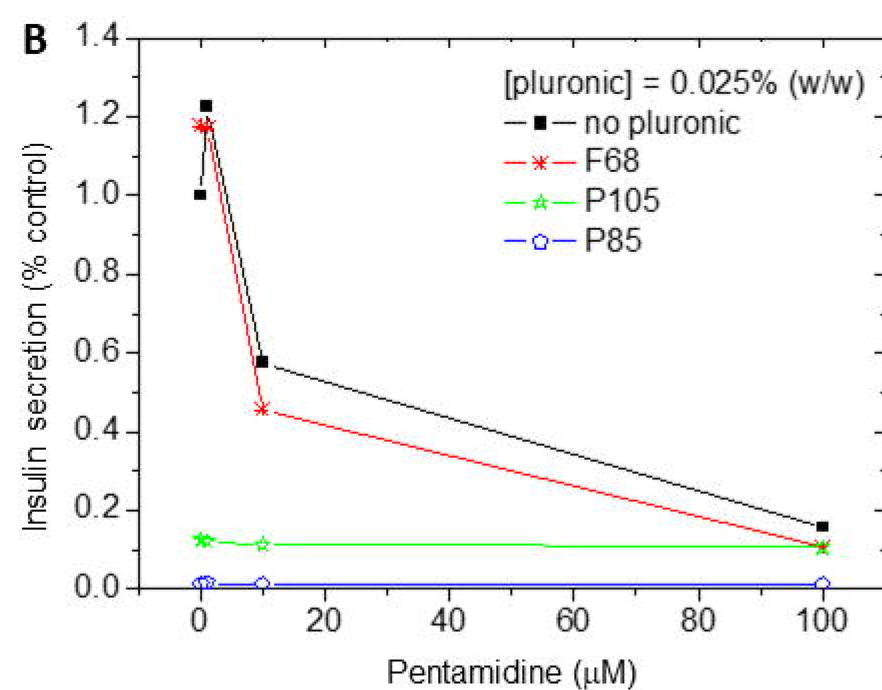
B
[pluronic] = 0.025% (w/w)
no pluronic
F68
P105
P85
Insulin secretion (% control)
Pentamidine (μM)

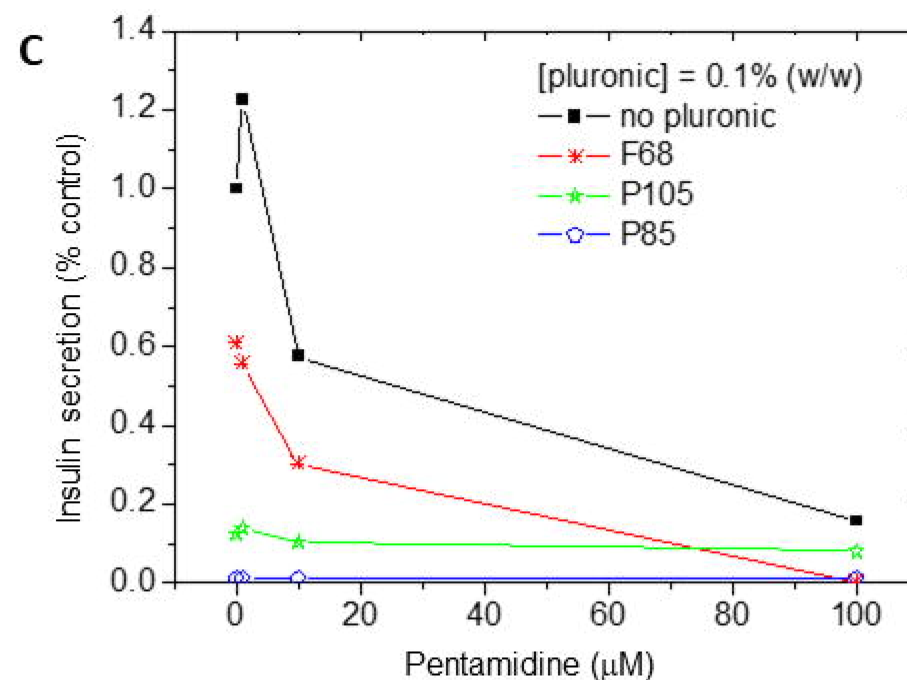
C
[pluronic] = 0.1% (w/w)
no pluronic
F68
P105
P85
Insulin secretion (% control)
Pentamidine (μM)

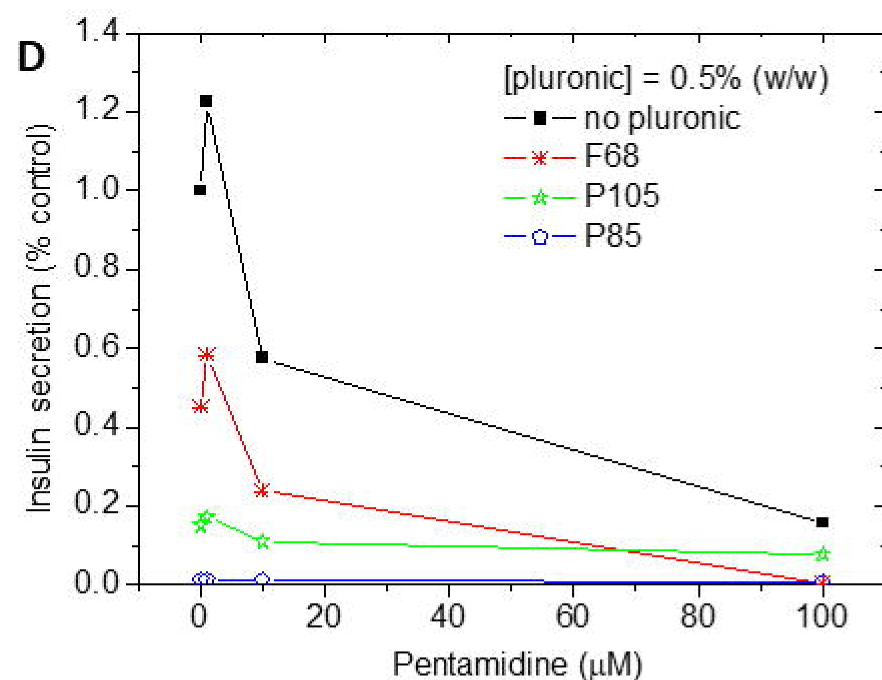
D
[pluronic] = 0.5% (w/w)
no pluronic
F68
P105
P85
Insulin secretion (% control)
Pentamidine (μM)

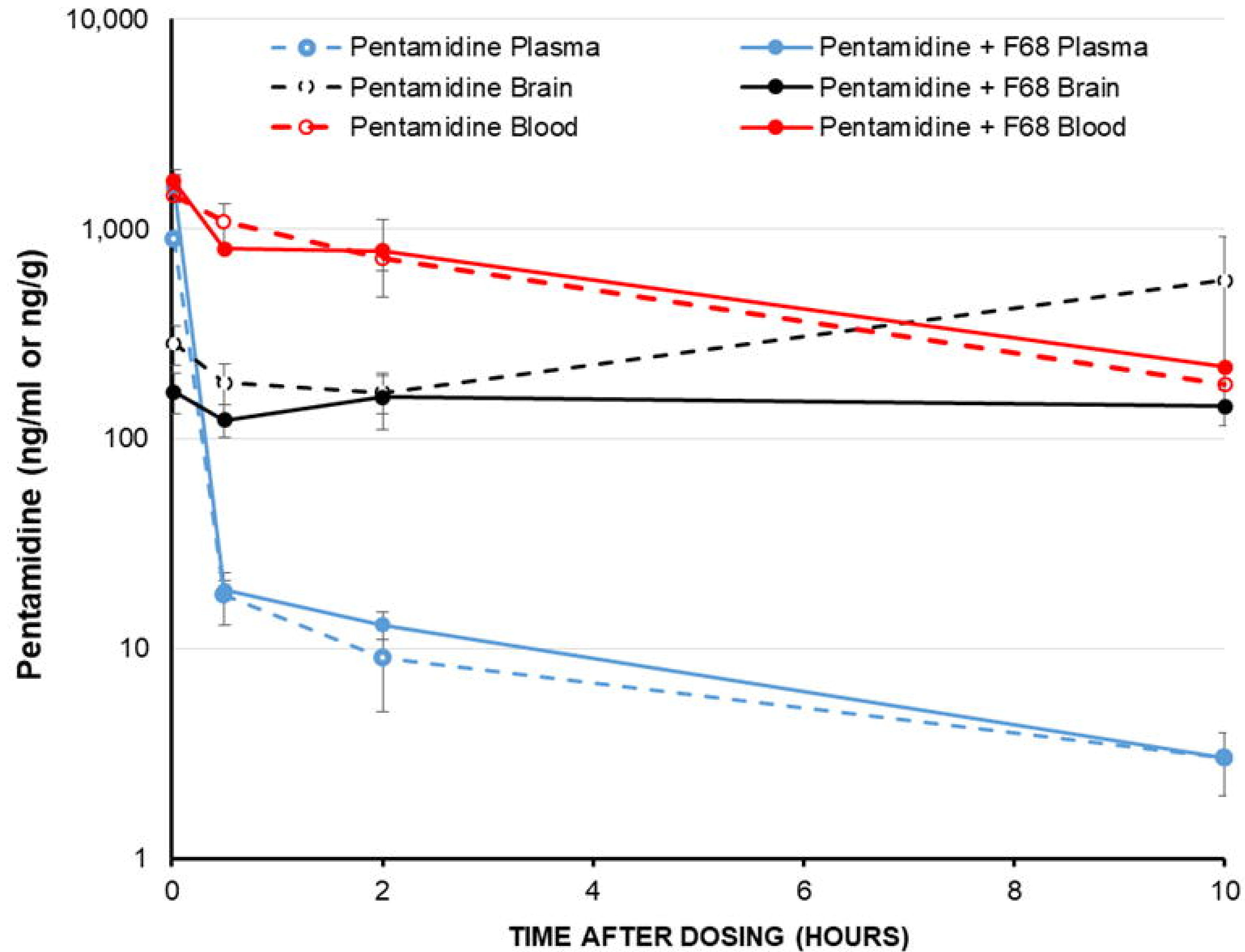

10,000
1,000
100
10
1
Pentamidine (ng/ml or ng/g)
Pentamidine Plasma
Pentamidine Brain
Pentamidine Blood
Pentamidine + F68 Plasma
Pentamidine + F68 Brain
Pentamidine + F68 Blood
0
2
4
6
8
10
TIME AFTER DOSING (HOURS)